Modified Salp Swarm Algorithm-Optimized Fractional-Order Adaptive Fuzzy PID Controller for Frequency Regulation of Hybrid Power System with Electric Vehicle

Debidasi Mohanty[1] · Sidhartha Panda[1]

Abstract

A considerable no. of intermittent renewable sources such as PV generation and wind energy when integrated to the conventional grid technology causes serious issues in the power systems like frequency instability. So a more balancing controller is desired for a stable and reliable operation of the power system. Bidirectional power control of the EV aggregator is making itself a wise choice for distributed energy storage to scale down the frequency and power fluctuation. In this work, an intelligent load frequency controller using a fractional-order adaptive fuzzy PID controller with filter (FOAFPIDF) for hybrid power system with electric vehicle (EV) based on modified salp swarm algorithm (MSSA) technique is proposed. The effectiveness of MSSA technique is compared with original salp swarm algorithm as well as moth flame optimization , grey wolf optimization , particle swarm optimization and sine cosine algorithm techniques for benchmark test functions using statistical analysis. The effectiveness of the suggested load frequency control strategy by the use of electric vehicle as well as with other energy storing elements such as the superconducting magnetic energy storage component, flywheel energy storage system and ultra-capacitor along with their inherent rate constraint nonlinearity is validated by numerical simulations conducted on the studied test system. It is demonstrated that the proposed controller provides a better control action to suppress the frequency fluctuations as compared to PID controller. The robustness of the controller is also investigated against variation of system parameters and random load changes.

Keywords Hybrid power system (HPS) · Load frequency control (LFC) · Salp swarm algorithm (SSA) · Fractional-order adaptive fuzzy PID controller with filter (FOAFPIDF) · Electric vehicle (EV)

Abbreviations

n	No. of variables
F	Food source
l	Current iteration
L	Maximum no. of iteration
K_{PV}	Gain of photovoltaic system
T_{PV}	Time constant of photovoltaic system
K_{WTG}	Gain of WTG
T_{WTG}	Time constant of WTG
K_{AE}	Gain of aqua electrolyser
T_{AE}	Time constant of aqua electrolyser
K_{FC}	Gain of FC
T_{FC}	Time constant of FC
K_{DEG}	Gain of DEG
T_{DEG}	Time constant of DEG
K_{FESS}	Gain of FESS
T_{FESS}	Time constant of FESS
K_{UC}	Gain of ultra-capacitor
T_{UC}	Time constant of ultra-capacitor
K_{SMES}	Gain of BESS
K_{SMES}	Time constant of BESS
K_{EV}	Gain of EV
T_{EV}	Time constant of EV
V_W	Wind speed
φ	Solar radiation
D	Damping constant
M	Inertia constant
Δf	Frequency deviation
u	Control signal
P_{PV}	Photovoltaic power output
P_{WTG}	Wind turbine generator output
P_L	Load demand

✉ Sidhartha Panda
panda_sidhartha@rediffmail.com

1   Department of Electrical Engineering, VSSUT, Burla,
    Odisha 768018, India

P_{FESS}	FESS power output
P_{SMES}	SMES power output
P_{EV}	Electric vehicle power output
P_{UC}	Ultra-capacitor power output
PU	Per unit

1 Introduction

The environmental pollutions, growing load, deregulation of the energy sector and rising costs of electricity transmission are making the renewable sources an attractive choice for the modern power system (Pan and Das 2016a; Ray et al. 2010, 2011; Lee and Wang 2008). This framework gives rise to a noble power system concept called hybrid power system (HPS). It is an amalgamation of renewables (wind turbine generators (WTG), solar photovoltaic (PV), etc.) units along with distributed energy resources (DERs) (fuel cell (FC), diesel energy generator (DEG)) and energy storing elements (flywheels, superconducting magnetic energy system, ultra-capacitors, etc.) and cluster of loads (Pan and Das 2016a; Ray et al. 2010). Due to scarcity of fossil fuels and the gradual progression in the innovation, wind energy and photovoltaic are making themselves a strong component for the hybrid power system. But the renewable sources show an extremely unpredictable behaviour due to varied environmental conditions. Thus, the sustainable generations and stochastic nature of the demand cause wide variations in the system frequency (Pan and Das 2016a). More or less the energy storing elements like flywheel energy storage system (FESS), superconducting magnetic energy storage (SMES) and ultra-capacitor (UC) are always recommended to couple to the system as a solution to minimize the generation and demand imbalance. The energy storage elements absorb/deliver the excess/shortfall active power to compensate any mismatch between generation and load (Pan and Das 2016b, 2015). Nevertheless the elevated price of energy storing components is forcing the engineers to consider about substitute of a fraction of energy storage components without affecting the system performance (Masuta and Yokoyama 2012). Thus, integration of electric vehicle (EVs) concept into the system has been gaining interest presently.

The electric vehicles are largely installed at the customer side. With the vehicle to grid (V2G) concept, the bidirectional charging and discharging of energy stored in the EV aggregator can be utilized to rapidly suppress the grid frequency fluctuations due to any kind of disturbances (Pahasa and Ngamroo 2015). EV aggregator is nothing but a relatively large no of electric vehicles which have taken part in the frequency regulation for a given hybrid power system structure (Ko and Sung 2017). So it is highly required that the challenges due to incorporation of adequate no. of EVs to the power system for load frequency control action must

be explored. A considerable no. of research papers has been published relevant to the contribution of EVs for auxiliary services. Authors in Ko and Sung (2017) have suggested an advanced control LFC method for power systems integrated with EVs by the traditional PI controller. On the other hand, the PI controller's performance is not satisfactory under large disturbance. The effect of time-varying delays on LFC systems has also reported in Ko and Sung (2017). In Datta and Senjyu (2013), LFC of power system with PV and EVs has been suggested by fuzzy logic controller (FLC). But it involves larger computational time due to complex design of membership functions. A fractional-order (FO) PID structure for power system incorporated with EVs is given in (Debbarma and Dutta 2016a). In Vachirasricirikul and Ngamroo (2014), a H_2/H_∞-based PI was proposed for frequency control in the smart grid using V2G concept. In Pahasa and Ngamroo (2015), authors have reported a multiple model predictive controller for controlling, charging and discharging state of charge (SOC) of EVs for frequency and power regulation of the microgrid system. But the robustness of the controller is not demonstrated in Pahasa and Ngamroo (2015). H_∞ controller in a power system with EV aggregator has been proposed in Pham et al. (2017) for primary as well as secondary frequency control action. In Masuta and Yokoyama (2012), Ali et al. (2014), the heat pump water heaters (HPWHs) and EVs are included in system as regulated loads for LFC. A hierarchical model predictive control (HiMPC) for LFC of smart grid incorporated with EVs is suggested in Kennel et al. (2013). This paper introduces a new adaptive approach known as fractional-order adaptive fuzzy PID controller with filter (FOAFPIDF) for robust frequency regulation of the hybrid power system with EV.

EVs update their real-time data information from the control signal through a communication infrastructure. The communication infrastructure comprises power line communication, wireless protocol, Bluetooth, etc. So there always exists a network-induced delay in the communication channel which can't be ignored while doing numerical simulations as it strongly affects the performance of the system. Hence, a time delay is considered for all the analysis in this study.

Fuzzy logic controller (FLC) is profoundly used in recent years because of its superiority in a large range of control-related tasks. FLC was first used by Mamdani for controlling a steam engine (Mamdani 1974). Over the years, FLC has become a robust controller than the conventional controllers because of its less sensitive behaviour during any dynamical changes in the system. But FLC suffers a disadvantage of no predefined standards for any specific application. It depends on the researcher's expertise and knowledge about the system. So a more advanced FLC technique is always welcomed. Practically, the system parameters may be abruptly changed

due to varied operating conditions. Therefore, effectiveness of the projected controller with uncertainties and random load changes is also taken into account for further consideration.

Salp swarm algorithm (SSA) has been a newly suggested optimization technique inspired by the swarming behaviour of the salps (Mirjalili et al. 2017). Salps form a salp chain in order to reach the desired location by continuously changing their position. The superiority of the SSA technique over some well-known techniques such as genetic algorithm (GA), particle swarm optimization (PSO), flower pollination algorithm (FPA), gravitational search algorithm (GSA), state of matter search (SMS), bat algorithm (BA) and firefly algorithm (FA) has reported in the literature (Mirjalili et al. 2017). In population-based algorithms, an adequate equilibrium among exploration and exploitation phases of the algorithm should be achieved to avoid local optima. In this paper, an approach has been developed to balance these two stages of the original SSA to achieve a higher quality solution.

In the original SSA technique, the convergence constant parameter (c_1) is varied slowly in early stages of iterations and rapidly in final iterations which degrades the exploration capability of the algorithm. The equation used to calculate c_1 is appropriately modified to overcome the shortcomings of the original SSA technique. Again in SSA technique, the position of the follower salp is determined from its previous position as well as neighbourhood salp's position. This results in more computational time and more memory requirement. This also increases the chances of random movement of any salp due to random movement of the neighbouring salp. The expression for updating the position of follower salp is also modified in such a way that the subsequent position of the salp is always determined from its previous position only. The modification decreases the computational time required by the algorithm with a minimum memory requirement to reach at the optimum position. The effectiveness of the proposed MSSA technique over original SSA in terms of result superiority and execution time is demonstrated. Proposed MSSA technique has also been compared with SSA and other alike meta-heuristic methods like moth flame optimization (MFO), grey wolf optimization (GWO), particle swarm optimization (PSO) and sine cosine algorithm (SCA).

The major offerings of the study include:

1. To suggest a modified SSA (MSSA) technique and exhibit its efficiency over the original SSA technique as well as other acknowledged optimization techniques like MFO, GWO, PSO and SCA in test functions.
2. To propose a FO adaptive fuzzy PID with filter (FOAF-PIDF) as load frequency controller for the studied hybrid power system.

3. To assess the effectiveness of MSSA-based FOAFPIDF controller with that of MSSA-optimized classical PID controller.

The structure of the portions of the work is provided here. Overview of the salp swarm algorithm (SSA) algorithm is explained in Sect. 2. Section 3 explains the modification that is made on the MFO algorithm. Section 4 explains the individual components of the hybrid power system. Section 5 gives an introduction to the proposed FOAFPIDF controller designed for LFC approach. The objective function which is considered for the simulation purpose is briefly introduced in Sect. 6. Results and discussion is discussed in Sect. 7. Section 8 covers the conclusion of the paper, followed by the references.

2 Salp Swarm Algorithm

The prime motivation of salp swarm technique is the swarming behaviour of the biggest swarms on the planet, i.e. salp (Mirjalili et al. 2017).It is believed that the navigating and foraging behaviour of the salps always aims to achieve the best promising location by a coordinated action.

The complete population of salp is broken up into leader and followers. The first position of the salp sequence is always occupied by the leader. The leader guides the other swarms. Other salps follow the leader indirectly or directly. The location of the salp is characterized by an n-dimensional search area where n is the no. of variables. The food source T is the target for the salp in the search boundary.

The position of the leader always represented by the equation given by,

$$x_j^1 = \begin{cases} T_j + c_1((ub_j - lb_j)c_2 + lb_j) & c_3 \geq 0.5 \\ T_j - c_1((ub_j - lb_j)c_2 + lb_j) & c_3 \leq 0.5 \end{cases}, \qquad (1)$$

where x_j^1 and T_j denote the positions the leader and food source in the j-th dimension. The leader updates its location with respect to the food source only. The lower and upper bound of j-th dimension are given by lb_j, ub_j. c_1, c_2 and c_3 are random numbers.

The coefficient c_1 balances the exploration and exploitation phases of SSA technique. It is considered as the most important parameter in SSA algorithm.

It is represented as

$$c_1 = 2e-\left(4i_c/I_M\right)^2, \qquad (2)$$

where i_c and I_M denotes the present iteration and the maximum no. of iteration, respectively.

c_2 and c_3 parameters are uniformly created arbitrary numbers in [0, 1]. They decide the step size and movement direction of leader salp.

The location of the other salps (i.e. followers) are updated by the equation given by

$$x_j^i = \frac{1}{2}at^2 + v_0 t. \tag{3}$$

Equation (3) is an equivalent of the Newton's law of motion where $i \geq 2$, t denotes time, v_0 denotes the initial speed. The parameters a and v_0 are found by: $a = \frac{v_{final}}{v_0}$ and $v_0 = \frac{x - x_0}{t}$. Considering $v_0 = 0$ and difference among iterations is equal to 1, Eq. (3) is modified as,

$$x_j^i = \frac{(x_j^i + x_j^{i-1})}{2} \quad i \geq 2 \tag{4}$$

x_j^i represents the location of the i-th follower in j-th dimension.

3 Modified Salp Swarm Algorithm

The proposed MSSA algorithm has the general frame as that of the original SSA algorithm given in Sect. 2, but two of its parameters were modified. While doing the modification, it is always kept in mind that there should be a perfect equilibrium among the exploration and exploitation phenomena. Exploration guarantees the variation of the search agent's position stochastically and effectively whereas finding the best among all implies exploitation capability of any optimization technique. A sound balance between the two accelerates the algorithm to arrive at the optimum for any objective function.

i) The movement/position of the leader is always an important factor for SSA algorithm which is ultimately depends on the coefficient c_1.

c_1 is given by

$$c_1 = K_1 e - \left(4i_c/I_M\right)^2, \tag{5}$$

where i_c and I_M represents the present iteration and the maximum no. of iteration, respectively. The value of K_1 is set as 2 for the original SSA algorithm which governs the movement of the leader salp related to the food source. A high value of K_1 may result in leader salp moving beyond the food source position. In the proposed MSSA algorithm K_1 is defined as 0.1. This makes the distribution of searched points more towards the end point than the start point. In original SSA, c_1 varies slowly during initial iterations and rapidly during final iterations. But any optimization algorithm expects a rapid variation of the search agents during initial stages of iterations (i.e. exploring

the search space initially) and a moderate variation of the search agents during final stages of iterations (i.e. exploiting the search space locally). Again the value of c_1 during final iteration is higher in SSA as compared to MSSA which is making a larger deviation of the leader's position from the food source. As the other salps just follow the leader, they also face the same situation. These problems are also nullified with our newly modified value of K_1 by the much lower value of c_1 during last iteration.

Pseudo code for MSSA algorithm.

```
Initialize the population size, maximum no. of iteration (L), lower bound and upper bound
While (stop condition is not fulfilled)
Determine the fitness of all salp
T = location of the best salp
Evaluate c₁ using Eq.(5)
    for each salp (xᵢ)
        if (i==1)
            Evaluate Eq.(1)to determine the position of leader salp
        else
            Evaluate Eq.(4) to determine the position of follower salp
        end
    end
Adjust the salps as per the lower and upper ranges of variables
end
return T
```

(2) The location of the follower salp is formulated as follows:

$$x_j^i = \frac{1}{2}\left(x_j^i + x_j^{i-1}\right) \quad i \geq 2, \tag{6}$$

where x_j^i and x_j^{i-1} are the locations of i-th and $(i$-1)-th salps in j-th dimension. This ultimately requires storing the location of i-th and $(i$-1)-th salp after each iteration for computing the next location of i-th salp. It results in more computational time as well as more memory requirement. It is worth mentioning that the position of any follower salp is only dependent on its previous position not on its neighbouring salp position. It has a direct effect on the exploitation capacity of the technique as it prevents the random movement of any follower salp due to the random movement of neighbouring salp. Equation (6) in SSA technique is modified in MSSA technique and given by

$$x_j^i = \frac{1}{4}(x_j^i) \quad i \geq 2. \tag{7}$$

The modified equation decreases the execution time as there is no need to save the neighbourhood follower salp's position. This in turn improves the exploitation property of the algorithm.

4 Details of Studied System

The hybrid power system (HPS) proposed in the present work is a realistic system which includes solar and wind energy. Various energy storage components are integrated

with the distributed generations in HPS for a reliable supply to the load. As unpredictable characteristics of the wind and PV power output may lower the dimension of the energy storage elements, fuel cell is incorporated with the energy storing elements like EV, SMES, FESS and UC in the studied power system to overcome the stability associated problems. The EV, DEG and FC have higher time constants as compared to SMES, FESS and UC. Therefore, the response of the later units to the control signal becomes faster as compared to the former ones. So the overall system dynamics is maintained by the relative values of the time constants and gains of various units. Since all the essential dynamics required for the frequency stability studies have been included, general conclusions can be made from the results shown in the paper so as to carry out the suggested approach in an actual power system. Similar power systems have been extensively used in reference (Pan and Das 2016a, 2016b, 2015) for frequency control studies. The schematic and the transfer function modelling of the proposed HPS using different generations and energy storage are given in Figs. 1 and 2 correspondingly. The parameter values of each component are listed in Table 1. The generation subsystem includes two WTGs, one PV, two FCs and one DEG. One from each storage component SMES, FESS, EV and UC are connected to the load side.

4.1 Modelling of Generation Sources

The PV, FC, DEG and WTG are modelled by linear first-order transfer functions (Eqs. 8–11) with their corresponding gains (K_{PV}, K_{FC}, K_{DEG}, K_{WTG}) and time constants (T_{PV}, T_{FC}, T_{DEG}, T_{WTG}) reported in Table 1 (Pan and Das 2016a, 2016b). n represents the no of units of each source.

$$G_{PV}(s) = \frac{K_{PV}}{1 + sT_{PV}} = \frac{\Delta P_{PV}}{\Delta \varphi} \tag{8}$$

$$G_{FC_K}(s) = \frac{K_{FC}}{1 + sT_{FC}} = \frac{\Delta P_{FC}}{\Delta P_{AE}} n = 1, 2 \tag{9}$$

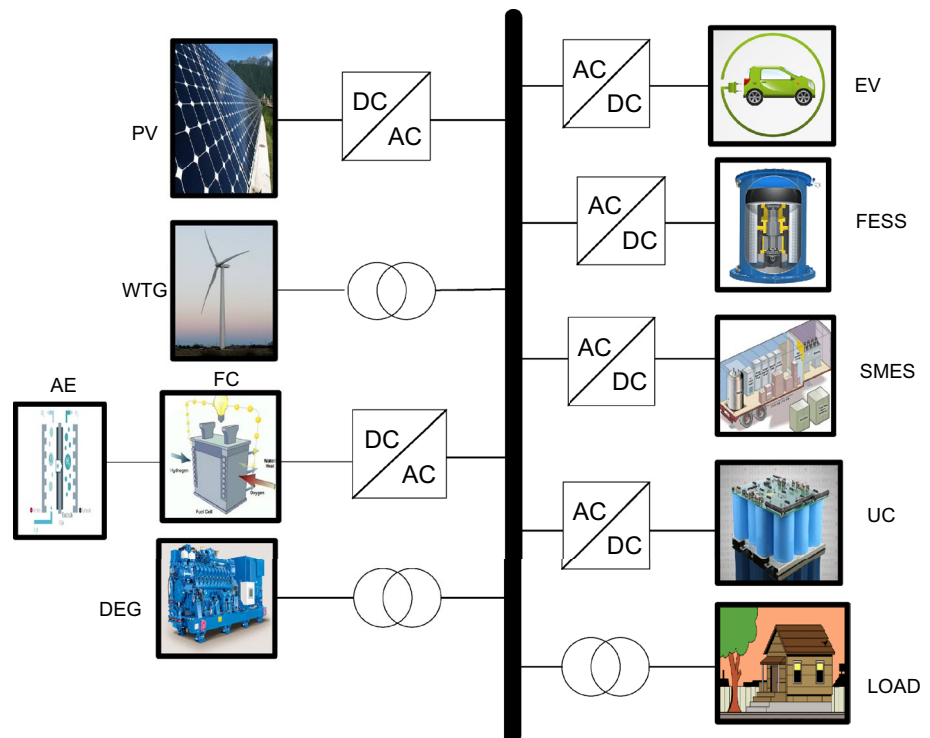$$G_{DEG}(s) = \frac{K_{DEG}}{1 + sT_{DEG}} = \frac{\Delta P_{DEG}}{\Delta u} \tag{10}$$

$$G_{WTG_K}(s) = \frac{K_{WTG}}{1 + sT_{WTG}} = \frac{\Delta P_{WTG}}{\Delta P_W} n = 1, 2. \tag{11}$$

The mathematical modelling of HPS parameters is described as below.

4.1.1 Wind Turbine Modelling

The wind turbine power (Pan and Das 2016a) is specified by
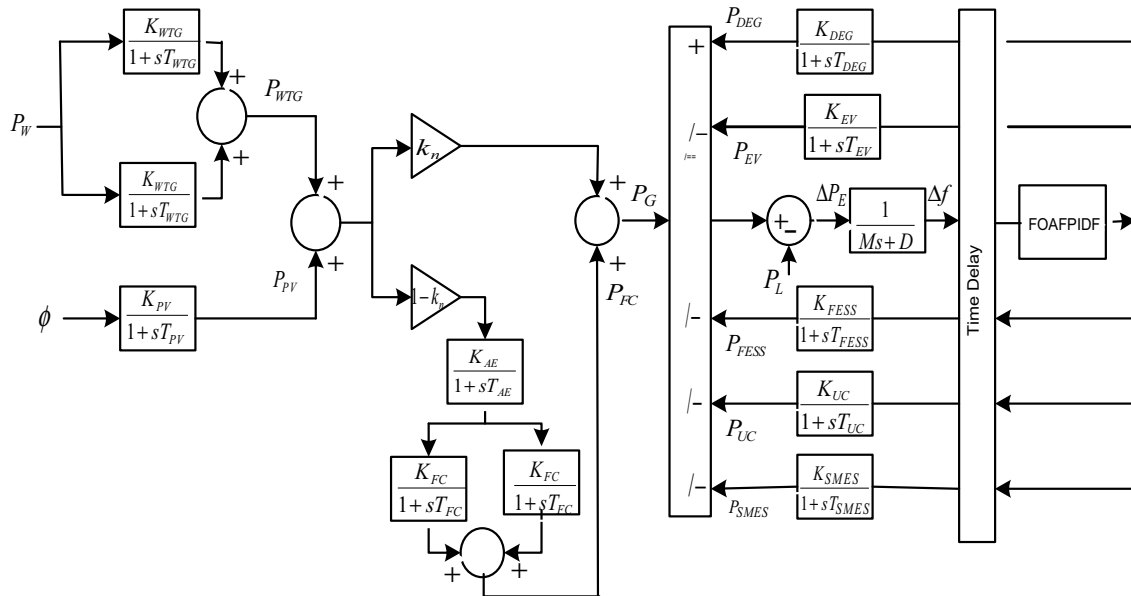
Fig. 1 Configuration of the proposed HPS

Fig. 2 Block diagram representation of the studied HPS with LFC

Table 1 Normalized Specification of studied system

Systems	Parameter values	
Solar Photovoltaic (PV)	$K_{PV} = 1$	$T_{PV} = 1.8$
Wind Turbine Generator (WTG)	$K_{WTG} = 1$	$T_{WTG} = 1$
Diesel Energy Generator (DEG)	$K_{DEG} = 0.003$	$T_{DEG} = 2$
Superconducting magnetic energy storage (SMES)	$K_{SMES} = -0.12$	$T_{SMES} = 0.03$
Flywheel Energy Storage System (FESS)	$K_{FESS} = -0.01$	$T_{FESS} = 0.1$
Ultra-capacitor (UC)	$K_{UC} = -0.7$	$T_{UC} = 0.9$
Electric Vehicle (EV)	$K_{EV} = 1$	$T_{EV} = 1$
Fuel Cell (FC)	$K_{FC} = 0.01$	$T_{FC} = 4$
Aqua Electrolyser (AE)	$K_{AE} = 0.002$	$T_{AE} = 0.5$

$$P_W = \frac{1}{2} \times C_P \times A_r \times \rho \times V_W^3, \tag{12}$$

where $\rho = 1.250$ kg/m^2 is the density of air and $A_r = 1735$ m^2 is the blade swept area.

The wind turbine power coefficient (C_P) (Pan and Das 2016a) is related to blade pitch angle (β) and tip speed ratio (λ) and characterized by:

$$C_p = (0.44 - 0.0167\beta) \sin\left[\frac{\pi(\lambda - 3)}{15 - 0.3\beta}\right]$$
$$- 0.0184(\lambda - 3)\beta \quad \beta = 0.1745. \tag{13}$$

λ is given by

$$\lambda = \frac{R_{blade} * \omega_{blade}}{V_W}, \tag{14}$$

where rotational speed $\omega_{blade} = 3.14$ rad per second radius $R_{blade} = 23.5$ m.

V_W is represented by

$$V_W = 7.5\varphi_H(t) - \varphi_H(t - 20), \tag{15}$$

where $\varphi_H(t)$ is the Heaviside function.

4.1.2 Modelling of Photovoltaic Power

The PV system output power (Pan and Das 2016a) is given by

$$P_{PV} = \eta S\varphi[1 - 0.005 \times (T + 25)], \tag{16}$$

where $S(= 4084$ m^2), is surface area of the PV array, η ($= 10\%$) is the efficiency of the PV cells, φ is the solar radiation in kw/m^2 and $T(= 25$ °C) is the ambient temperature.

φ is expressed as

$$\varphi = 0.5\varphi_H(t) - 0.3\varphi_H(t-20). \tag{17}$$

4.2 Aqua Electrolyser Modelling

The aqua electrolyser is modelled as in Eq. (18). AE utilizes a portion, i.e. $(1 - k_n)$ of the generated renewable power and releases hydrogen as required by the fuel cell (Pan and Das 2016a; Ray et al. 2011).

$$G_{AE}(s) = \frac{K_{AE}}{1 + sT_{AE}} \tag{18}$$

k_n is set as 0.6 here.

4.3 Modelling of Energy Storage Components

Energy storing elements such as FESS, SMES and UC effectively acquire the surplus active power from the renewable sources and make it available to the load during generation deficiency for a stable hybrid system operation (Pan and Das 2016a, 2016b; Ray et al. 2011; Pothiya and Issarachai 2008).

FESS, SMES and UC are the three storage systems considered in the paper which are controlled by the LFC controller and are expressed as

$$G_{FESS}(s) = \frac{K_{FESS}}{1 + sT_{FESS}} \tag{19}$$

$$G_{SMES}(s) = \frac{K_{SMES}}{1 + sT_{SMES}} \tag{20}$$

$$G_{UC}(s) = \frac{K_{UC}}{1 + sT_{UC}}. \tag{21}$$

4.4 Modelling of EV Aggregator

EV aggregator consists of a large no. of EVs. The model of an EV is usually represented by transfer function as (Ko and Sung 2017):

$$G_{EV}(s) = \frac{K_{EV}}{1 + sT_{EV}}, \tag{22}$$

where K_{EV} and T_{EV} denotes the gain and time constant of the EV system.

Energy storage elements are supplied with rate constraint nonlinearity as shown in Fig. 3 to inhibit the mechanical jerk because of rapid frequency fluctuation (Pan and Das 2016b, 2015). Their rate constraint nonlinearities are given by: $|P_{SMES}| < 0.01, |P_{FESS}| < 0.09, |P_{UC}| < 1.2, |P_{DEG}| < 0.09$ and $|P_{EV}| < 0.15$. This is again a practical scenario as this will prevent any energy storing unit to store or release power very fast.

4.5 Characteristic of Load Demand

The variations in the load demand P_L can be formulated as

$$P_L = 0.6\varphi_H(t) - 0.3\varphi_H(t-20) - 0.1\varphi_H(t-40). \tag{23}$$

4.6 Modelling of Power System

In HPS, when the generating power (P_G) deviate from the load demand (P_L), the frequency fluctuates depending on their difference. When the power deviation is more, the frequency fluctuation is more and vice versa. So the frequency deviation (Δf) is an inherent function of power deviation (ΔP_E). There also exists a time delay between ΔP_E and Δf, thus $\Delta f / \Delta P_E$ is characterized by a simple expression given by (Senjyu et al. 2005)

$$G_{sys}(s) = \frac{\Delta f}{\Delta P_E} = \frac{1}{Ms + D}, \tag{24}$$

where D (0.03) is the damping constant of the HPS which represents all the damping components (due to speed governing, excitation, due to turbine generator, etc.) (Agrawal et al. 1999). M (0.4) is the inertia values that represent equivalent mass of rotating components present in the HPS (Zhang and Xu 2017).

5 Design of Controller Structure

5.1 Fractional-Order PID Controller (FOPID)

Classical PID structure is employed in most cases due to its simple design and cost effectiveness. But, the performance of the controller is greatly affected when the system is of

Fig. 3 Rate constraint type nonlinearity for an energy storing element having a gain of K and time constant of T
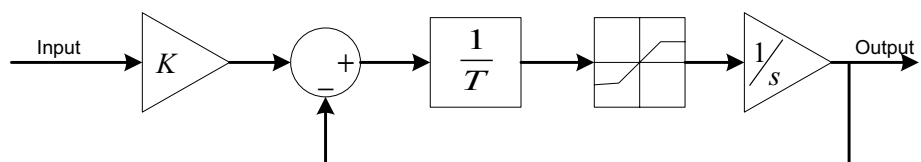
higher order with considerable nonlinearity and uncertainties. Fractional-order PID controllers have been receiving a wide attention among the researchers because of its design flexibility and dynamic stability. In fractional calculus concept, integer order differentiation and integration are replaced by fractional orders (Debbarma and Dutta 2016b; Taher et al. 2014; Alomoush 2010). The fractional parts offer additional degrees of freedom in designing the controller (Taher et al. 2014). In the present discussion on fractional calculus, the fractional operator $(_aD_t^q)$ denotes fractional differentiation or integration based on the sign of q. It is defined as

$$
_aD_t^q = \begin{cases} \dfrac{d^q}{dt^q} & q > 0 \\ 1 & q = 0 \\ \int\limits_a^t d\tau^{-q} & q < 0 \end{cases},
\tag{25}
$$

where operational boundaries are a and t fractional order is represented by q.

As per Riemann–Liouville (RL) description, the fractional derivative of order α is represented by

$$
_aD_t^\alpha f(t) = \frac{1}{\Gamma(n-\alpha)} \frac{d^n}{dt^n} \int\limits_0^t (t-\tau)^{n-\alpha-1} f(\tau) d\tau \quad n-1 \le \alpha \le n.
\tag{26}
$$

And the fractional integral of order α is given by

$$
_aD_t^{-\alpha} f(t) = \frac{1}{\Gamma(\alpha)} \int\limits_a^t (t-\tau)^{\alpha-1} f(\tau) d\tau,
\tag{27}
$$

where $_aD_t^\alpha$ is the fractional operative, n is an integer and $\Gamma(.)$ is the Euler's gamma expression.

The Laplace transformation of E q. (27) is given by

$$
L\{_aD_t^\alpha f(t)\} = s^\alpha F(s) - \sum_{k=0}^{n-1} s_a^k D_t^{\alpha-k-1} f(t)|_{t=0}.
\tag{28}
$$

When zero initial condition, the system with dynamic characteristic is given by differential equations of fractional derivative, having a transfer function representation of fractional order of s. Our work includes the CRONE estimation, which means robust fractional-order control is formulated by

$$
S^\alpha \approx G \prod_{n=1}^{N} \frac{1 + \frac{s}{\omega_{z,n}}}{1 + \frac{s}{\omega_{p,n}}},
\tag{29}
$$

where G represents the variable gain. The general type of FO controller is specified by $PI^\lambda D^\mu$ as:

$$
G(s) = K_P + K_D s^\mu + \frac{K_I}{s^\lambda},
\tag{30}
$$

where K_P, K_D and K_I are gains of PID. Also μ and λ are order of the differentiator and integrator, respectively.

5.2 Fractional-Order Adaptive Fuzzy PIDF Controller

Adaptive fuzzy-based PID controller has now gaining lots of attention among the researchers and numerous methods are being proposed in (Savran and Kahraman 2014) and (Woo et al. 2000). The controller structure of adaptive fuzzy PID controller with filter (FOAFPIDF) is shown in Fig. 4. A FLC has a group of specified rules (Fereidouni et al. 2015). The design of FLC is based on the determination of the linguistic variables of the input/output membership functions (MFs), determination of the input/output scaling factors (SFs) and controller gains. The performance of FLC system can be improved by rule and MF tuning which is a complicated job and may require precise configurations by a specialist for implementation. On the other hand, gain tuning approach
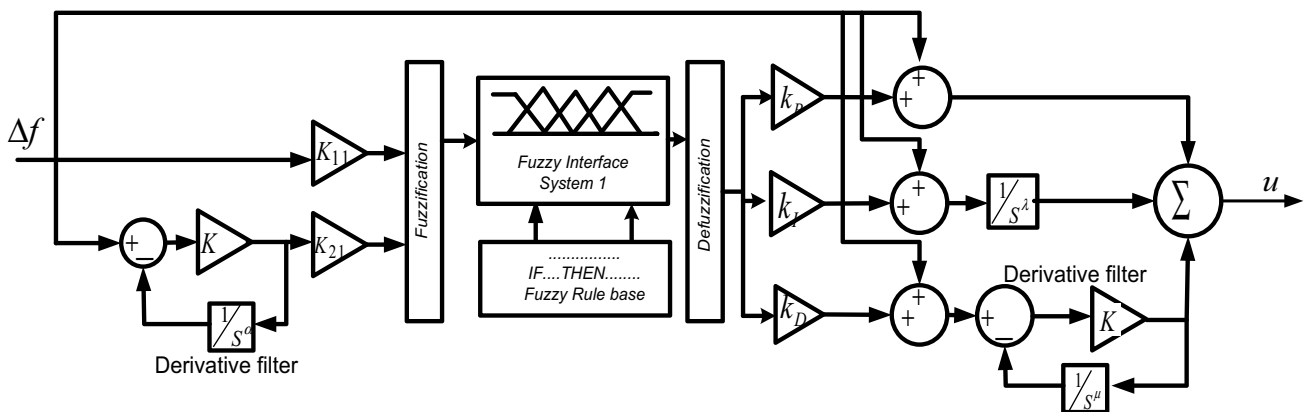

Fig. 4 Proposed FOAFPIDF controller

is the universal method of designing the FLC system where universal rule base and typical MF's can be engaged for diverse purpose and SFs can be adjusted for optimal FLC system. In this study, fuzzy gain tuning method is employed which can be generalized for others cases simply by retuning the scaling factors. For proper control action, the MFs should be a nonlinear function of frequency deviation (Δf) and derivative of frequency deviation ($\Delta \dot{f}$). In conventional FLC, this nonlinearity is generally accomplished by a fixed no. of IF–THEN rules. In the proposed strategy a FOAF-PIDF controller is used for continuously computing the output SFs to make the system optimally controlled depending on inputs (Δf and $\Delta \dot{f}$).

The configuration of the proposed FOAFPIDF is presented in Fig. 4. Derivative mode increases speed of the controller response and improves stability of the system. But it may give rise to unreasonable size control output particularly if the input signal has huge deviations around the nominal value and contains noise. In this context, a first-order filter is placed on the derivative term so that the disturbance due to the noise is avoided as frequency noise is attenuated. For easy implementation, same MFs for the inputs (error and its derivative) and output are considered as depicted in Fig. 5. The MFs are fixed to be triangular which is versatile and economical for real-time applications than other MFs. For the present study, Mamdani fuzzy interface is considered. Table 2 shows the five fuzzy linguistic variables Negative high, Negative low, Zero, Positive low and Positive high which are symbolized as N_H, N_L, Z, P_L and P_H, respectively, employed for the proposed controller design. The input SFs (K_{11}, K_{21}), order of input derivative filter (α), output SFs (K_P, K_I, K_D), order of output derivative filter (μ), order of input integrator (λ) of FOAFPIDF controller is optimized by the MSSA technique. The value of K is fixed to 100 for the design of the controller.

Table 2 Linear rule base for FOAFPIDF controller

| Δf	$\Delta \dot{f}$				
	N_H	N_L	Z	P_L	P_H
N_H	N_H	N_H	N_L	N_L	Z
N_L	N_H	N_L	N_L	Z	P_L
Z	N_L	N_L	Z	P_L	P_L
P_L	N_L	Z	P_L	P_L	P_H
P_H	Z	P_L	P_L	P_L	P_H

6 Objective Function

For efficient performance of the optimization tuned controller design, objective function representation is important. Among all, integral of absolute error (IAE) reduces the contribution of large errors which occur early in time as well as penalizes the small errors (less than one) occurring later in the response. It also provides small overshoot as well as less settling time (Ranganayakulu et al. 2016).

The considered HPS was simulated by considering integral of absolute of two terms, i.e. frequency variation (Δf) and control signal output (u) given by

$$J = \int_0^{T_{max}} (|\Delta f(t)| + |u(t)|)dt, \quad (31)$$

where T_{max} is the maximum simulation time.

Fig. 5 Membership functions for Δf, $\Delta \dot{f}$ and output
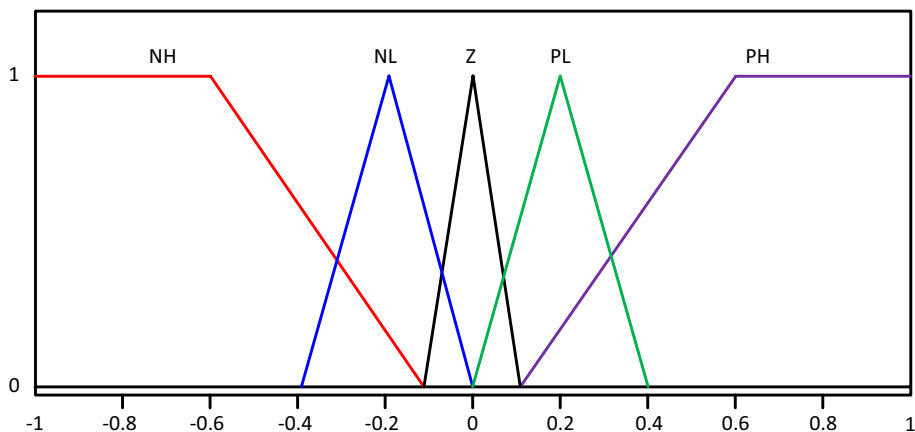
7 Results and Discussion

7.1 Performance Investigation of the MSSA Algorithm

The operation of the MSSA algorithm is benchmarked by considering 21 standard test functions (Mirjalili et al. 2014; Yao et al. 1999) in this sub-section. To evaluate the effectiveness of MSSA algorithm, results are compared with some recent well-known techniques such as moth flame optimization (MFO), grey wolf optimization (GWO), particle swarm optimization (PSO) and sine cosine algorithm (SCA) using 21 benchmark test functions. These benchmark functions comprise of unimodal as well as multimodal functions to authenticate the efficiency of the projected technique in getting the global optimum value. 30 no. of search agents and 1000 no. of maximum iterations are set for each function run. The no. of independent runs is set to 30. Table 3 lists these test functions with their range of the search area, dimensions (*Dim*) and optimum values ($f_{\min}$) for the investigation purpose.

The parameter setting of each algorithm is as follows:

(1) MFO (Mirjalili 2015): The convergence constant '*r*' is linearly reduced from -1 to -2.
(2) GWO (Mirjalili et al. 2014): The parameter '*a*' linearly decreased from [2, 0]. r_1, r_2 are taken as random number in [0, 1].
(3) PSO (Chaturvedi et al. 2009): Inertia weight (*w*) is fixed at 0.9. Cognitive acceleration (c_1) and social acceleration (c_2) randomly varied in [0, 2].
(4) SCA (Mirjalili 2016): $r_1, r_2, r_3 \in [0, 1]$ are random numbers and r_4 is taken as $0.5 \leq r_4 < 0.5$.

Table 4 contains the results like average (avg.) and standard deviation (std. dev.) of objective function values found in 30 runs. Among the considered benchmark test functions, f_1 to f_7 are unimodal functions. These are specially considered for testing the exploitation ability of the technique as they possess single global optima (Padhy et al. 2017). Table 4 clearly depicts that modified SSA offers statically significant better results in all the functions as compared to the SSA method. Suggested MSSA technique also shows substantially better results as compared to MFO, GWO, PSO and SCA methods. It is apparent from Table 4 that MSSA is superior to some of the well-known optimization techniques like SSA, MFO, GWO, PSO and SCA in terms of better exploitation capability. This proves that the modifications of the MSSA methods are capable to effectively enhance the exploitation capability of the given optimization technique. Out of 21 functions, the modified SSA technique shows a remarkable

better result for 18 of the functions when compared to the SSA algorithm and competitive results in the remaining 3 functions.

Functions f_8 to f_{13} are having higher no. of local optima and known as multimodal functions, thus making themselves suitable for investigating the exploration capability of an algorithm (Yao et al. 1999). It is noticed from Table 4 that MSSA algorithm outperforms than SSA, MFO and PSO algorithms in all these functions. For GWO and SCA algorithms, the modified SSA algorithm gives competitive results only in f_{13} and f_8 functions, respectively, and for rest of the test functions our proposed algorithm is proved to be better. It strongly proves that MSSA helps in improving exploration ability of original SSA and able to evade the local optima stagnations.

The functions f_{14} to f_{21} are multimodal functions with fewer local minima which are usually considered for simultaneous validation of both exploration and exploitation property of any optimization algorithm (Yao et al. 1999). Out of the 8 functions, the proposed algorithm yields better results for 5 of the functions and for f_{15} to f_{17}, the result remains equal to the SSA algorithm. Table 4 clearly receipts that the proposed modified MFO outperforms the MFO, PSO and SCA algorithms for all the benchmark functions. While comparing to GWO, our proposed algorithm only fails in f_{20} and f_{21} whereas gives improved results for rest of the functions.

Table 5 shows the computational time taken by MSSA and SSA technique for each function running at 30 times. The results clearly prove that the modifications made in the MSSA technique are able to reduce the execution time required by the algorithm than the SSA technique for all the functions.

The convergence characteristics, which show the best-obtained results for any given objective function optimized by the proposed MSSA and the original SSA, are given in Fig. 6. For the better illustration, the convergence characteristics with MSSA and SSA are zoomed for all test functions and given in Fig. 6. It is apparent from Fig. 6 that the MSSA outperforms the SSA technique in terms of faster convergence rate as well as better promising solutions. A nonparametric statistical test known as Wilcoxon's test (Cuevas et al. 2014) is considered here to compare the significance of our proposed technique with that of other techniques. The test is conducted for each algorithm by taking into account the best-obtained solution of each test function in 30 autonomous runs and a significance level of 95%. The results (*p* value) are shown in Table 6 for pair-wise comparison of the MSSA vs. SSA, MSSA vs. MFO, MSSA vs. GWO, MSSA vs. PSO and MSSA vs. SCA. An algorithm is highly significant when *p* value returns a value less than 0.05. It can be noticed from Table 6 that, for most of the functions (except in f_{13}, f_{18} while comparing to MFO and f_{13} while comparing

Table 3 Details of considered test functions

Test Function	Range	Dim	f_{min}
$f_1 = \sum_{i=1}^{n} x_i^2$	$[-100, 100]$	30	0
$f_2 = \sum_{i=1}^{n} |x_i| + \prod_{i=1}^{n} |x_i|$	$[-10, 10]$	30	0
$f_3 = \sum_{i=1}^{n} \left(\sum_{j=1}^{i} x_i \right)^2$	$[-100, 100]$	30	0
$f_4 = \max_i \{|x_i|, 1 \leq i \leq n\}$	$[-100, 100]$	30	0
$f_5 = \sum_{i=1}^{n-1} [100(x_{i+1} - x_i^2)^2 + (x_i - 1)^2]$	$[-30, 30]$	30	0
$f_6 = \sum_{i=1}^{n} \left([x_i + 0.5] \right)^2$	$[-100, 100]$	30	0
$f_7 = \sum_{i=1}^{n} i x^4 + random[0, 1]$	$[-1.28, 1.28]$	30	0
$f_8 = \sum_{i=1}^{n} -x_i \sin\left(\sqrt{|x_i|}\right)$	$[-500, 500]$	30	$-12{,}569.5$
$f_9 = \sum_{i=1}^{n} \left[x_i^2 - 10\cos(2\pi x_i) + 10 \right]^2$	$[-5.12, 5.12]$	30	0
$f_{10} = -20\exp\left(-0.2\sqrt{\frac{1}{n}\sum_{i=1}^{n} x_i^2}\right) - \exp(\frac{1}{n}\sum_{i=1}^{n}\cos 2\pi x_i) + 20 + e$	$[-32, 32]$	30	0
$f_{11} = \frac{1}{4000}\sum_{i=1}^{n} x_i^2 - \prod_{i=1}^{n}\cos(\frac{x_i}{\sqrt{i}}) + 1$	$[-600, 600]$	30	0
$f_{12} = \frac{\pi}{n}\left\{ 10\sin(\pi y_1) + \sum_{i=1}^{n-1}(y_i - 1)^2[1 + 10\sin^2(\pi y_{i+1}) + (y_n - 1)^2 \right\} + \sum_{i=1}^{n} u(x_i, 10, 100, 4)$ $y_i = 1 + \frac{x_i + 1}{4}$ $u(x_i, a, k, m) = \begin{cases} k(x_i - a)^m & x_i > a \\ 0 & -a < x_i < a \\ k(-x_i - a)^m & x_i < -a \end{cases}$	$[-50, 50]$	30	0
$f_{13} = 0.1\left\{ \sin^2(3\pi x_1)\sum_{i=1}^{n-1}(x_i - 1)^2[1 + \sin^2(3\pi x_{i+1})] + (x_n - 1)[1 + \sin^2(2\pi x_n)] \right\}$ $+ \sum_{i=1}^{n} u(x_i, 5, 100, 4)$	$[-50, 50]$	30	0
$f_{14} = \sum_{i=1}^{11}\left[a_i - \frac{x_1(b_i^2 + b_i x_2)}{b_i^2 + b_i x_3 + x_4} \right]^2$	$[-5, 5]$	4	0.0003
$f_{15} = 4x_1^2 - 2.1x_1^4 + \frac{1}{3}x_1^6 + x_1 x_2 - 4x_2^2 + 4x_2^4$	$[-5, 5]$	2	-1.0316
$f_{16} = \left(x_2 - \frac{5.1}{4\pi^2}x_1^2 + \frac{5}{\pi}x_1 - 6 \right)^2 + 10\left(1 - \frac{1}{8\pi} \right)\cos x_1 + 10$	$[-5, 5]$	2	0.398
$f_{17} = -\sum_{i=1}^{4} c_i \exp[-\sum_{j=1}^{3} a_{ij}(x_j - p_{ij})^2]$	$[1, 3]$	3	-3.86
$f_{18} = -\sum_{i=1}^{4} c_i \exp[-\sum_{j=1}^{6} a_{ij}(x_j - p_{ij})^2]$	$[0, 1]$	6	-3.32
$f_{19} = -\sum_{i=1}^{5}\left[(x - a_i)(x - a_i)^T + c_i \right]^{-1}$	$[0, 10]$	4	-10
$f_{20} = -\sum_{i=1}^{7}\left[(x - a_i)(x - a_i)^T + c_i \right]^{-1}$	$[0, 10]$	4	-10

Table 3 (continued)

Test Function	Range	Dim	f_{min}
$f_{21} = -\sum_{i=1}^{10} \left[(x - a_i)(x - a_i)^T + c_i \right]^{-1}$	[0, 10]	4	−10

Table 4 Statistical results of the MSSA and comparison with other techniques

Fun		MSSA	SSA	MFO	GWO	PSO	SCA
Unimodal functions							
f_1	Avg	0	0.125e−7	3.3333e+3	0.074e−57	1.3670e+3	0.0400
	Std dev	0	0.034e−7	4.7946e+3	0.132e−57	0.7290e+3	0.1301
f_2	Avg	0	1.284	35.0001	0.146e−33	17.5702	0.0661e−3
	Std dev	0	1.008	24.0330	0.317e−33	4.7127	0.2561e-3
f_3	Avg	0	268.759	2.0275e+4	0.232e−15	7.0816e+3	3.4530e+3
	Std dev	0	193.468	1.9357e+4	0.350e−15	2.7793e+3	3.4151e+3
f_4	Avg	0	6.999	67.3083	0.180e−13	20.7866	21.6945
	Std dev	0	2.878	9.5462	0.368e−13	3.6848	11.2530
f_5	Avg	28.43	104.964	2.4394e+4	27.132	1.3584e+5	0.5940e+3
	Std dev	0.0496	173.067	4.0288e+4	0.838	1.4392e+5	1.5391e+3
f_6	Avg	0.374e−10	0.117e−7	1.663e+3	0.568	1.0621e+3	4.8014
	Std dev	0.072e−10	0.029e−7	3.783e+3	0.338	0.4669e+3	0.8277
f_7	Avg	0.037e−3	0.1053	3.7722	0.895e−3	0.3047	0.0360
	Std dev	0.032e−3	0.0442	8.1114	0.508e-3	0.1358	0.0272
Multimodal functions with many local minima							
f_8	Avg	−7.233e+3	−7.6332e+3	−8.8157e+3	−6.028e+3	−2.5879e+52	−3.8821e+3
	Std dev	0.591e+3	0.8238e+3	0.8960e+3	0.728e+3	5.2760e+52	0.3317e+3
f_9	Avg	0	58.4371	158.4110	0.732	164.1679	18.4723
	Std dev	0	16.8200	42.7053	1.637	28.4501	25.8720
f_{10}	Avg	0.888e−15	2.0805	14.8338	0.151e−13	20.9196	15.0546
	Std dev	0.0e−15	0.9242	7.2912	0.013e−13	0.5878	8.3313
f_{11}	Avg	0	0.0103	27.1178	0.0007	1.3419	0.2145
	Std dev	0	0.0111	63.3808	0.0029	0.2048	0.1665
f_{12}	Avg	0.0486e−11	5.4054	1.2862	0.0365	1.0691e+3	1.6173e+3
	Std dev	0.0398e−11	2.5923	1.8394	0.0191	5.7075e+3	8.8475e+3
f_{13}	Avg	1.291	3.3742	1.367e+07	0.619	3.5652e+4	65.7842
	Std dev	1.489	8.8628	7.487e+07	0.242	6.7149e+4	305.8980
Multimodal functions with fewer local minima							
f_{14}	Avg	0.0005	0.0021	0.0032	0.0044	0.0011	0.9433e−3
	Std dev	0.0003	0.0050	0.0062	0.0081	0.0002	0.4066e−3
f_{15}	Avg	−1.0316	−1.0316	−1.0316	−1.0316	−1.0316	−1.0316
	Std dev	0.0000	0.0000	0.0000	0.000	0.0000	0.0000
f_{16}	Avg	0.3979	0.3979	0.3979	0.3979	0.3979	0.3990
	Std dev	0	0	0	0.000	0.0002	0.0013
f_{17}	avg	−3.8628	−3.8628	−3.8628	−3.861	−3.862	−3.8554
	Std dev	0.0000	0.0000	0.0000	0.003	2.58e-15	0.0026
f_{18}	avg	−3.2982	−3.2371	−3.2417	−3.265	−3.2869	−3.0054
	Std dev	0.0484	0.0566	0.0644	0.078	0.0592	0.1657
f_{19}	avg	−4.895	−7.808	−6.3868	−9.3092	−8.0528	−2.5257
	Std dev	0.608	3.224	3.2687	1.9185	2.4921	2.3084
f_{20}	avg	−5.465	−8.778	−8.378	−10.2253	−8.9810	−4.5886
	Std dev	1.773	3.040	3.211	0.9704	2.3944	2.1878
f_{21}	avg	−5.144	−9.318	−7.933	−10.5359	−9.3787	−4.2898
	Std dev	1.720	2.799	3.292	0.0002	2.2851	1.9946

Table 5 Computation time taken by MSSA and SSA technique for each function run

fun	MSSA	SSA	fun	MSSA	SSA	fun	MSSA	SSA	fun	MSSA	SSA
f_1	6.28157	6.41448	f_7	8.87582	9.86205	f_{13}	17.27259	17.79075	f_{21}	25.04151	25.89048
f_2	6.90661	7.00139	f_8	7.57328	7.82937	f_{14}	13.69218	13.79831	f_{22}	30.37835	30.91409
f_3	23.74488	24.17522	f_9	6.75625	7.04795	f_{15}	11.61178	11.92170	f_{23}	35.76742	36.87830
f_4	6.40529	6.44773	f_{10}	7.36254	7.62693	f_{16}	10.86891	11.48886			
f_5	7.18245	7.27580	f_{11}	8.19415	8.64485	f_{19}	17.47523	17.99831			
f_6	6.36467	6.40772	f_{12}	17.71690	17.83831	f_{20}	17.75246	18.36637			

to GWO), p value is quite less than 0.05. This implies that the MSSA is significant in achieving the best promising solutions for unimodal as well as multimodal functions.

7.2 Controller Performance in Hybrid Power System

The suggested HPS has been implemented in MATLAB 9.0.0.341363 (R2016a) environment. The model (Fig. 2) is developed using SIMULINK library with the parameters of the HPS as given in Table 1 and the optimization techniques (SSA, MSSA) are written in .m files. The components of the HPS are assumed to be functioning with their corresponding rate constraint nonlinearities as given in Sect. 4.3. To examine the efficiency of the proposed approach for frequency control of HPS, both PID and FOAFPIDF controllers are tuned employing SSA and MSSA method. The searching limits for $K_{11}, K_{21}, K_P, K_I, K_D, \lambda, \mu, \alpha$ are set as $[0.001\ 1]$ for both the controller (Pan and Das 2016b). The system is run repeatedly with a maximum iteration of 50 until the best optimized result is found out. Initially the controller parameters are found by considering case 1 and further the same parameter values are applied to other cases to validate its effectiveness. Table 7 provides the tuned values of the PID and the FOAFPIDF. It can be seen from Table 7 that minimum objective function value ($J = 4.0846$) is attained with suggested MSSA tuned FOAFPIDF as compared to SSA tuned FOAFPIDF ($J = 4.3420$), MSSA tuned PID ($J = 5.1948$) and SSA tuned PID ($J = 5.3329$). This proves the superiority of the modified SSA technique over SSA technique.

Various cases are undertaken to assess the effectiveness of proposed controller:

7.3 Case 1:

In this case, the proposed system is simulated with steady wind and PV power output of 0.43 pu and 0.51 pu, respectively, for $0 \leq t \leq 20$ s (Fig. 7). A constant load demand of 0.6 pu occurs during that period. The system parameters are set at their nominal value. The frequency deviation characteristics of both the controllers optimized by SSA and MSSA method are given in Fig. 8. The figure evidently

demonstrates that the MSSA-optimized proposed controller achieves an efficient damping for frequency deviation as related to the other schemes. The PID controller (both SSA and MSSA tuned) takes more than 12 s and the SSA-optimized FOAFPIDF controller takes approximately 8 s to reach the steady position. However, MSSA tuned fractional-order adaptive fuzzy PIDF controller (FOAFPIDF) controller makes it within 5 s. This establishes the superiority of the proposed FOAFPIDF on the hybrid power system. After 20 s, both wind and PV power outputs reduce from 0.43 pu to 0.35 pu and 0.51 pu to 0.2 pu in that order with the demand changes to 0.3 pu till 40 s. The system starts fluctuating owing to these abrupt variations in power. This deviation is regulated by both PID and FOAFPIDF such that the error in demand and supply is minimized. For the above mentioned situation, the MSSA-optimized FOAFPIDF controller acts faster with less overshoot and

minimizes the frequency deviation very effectively as compared to the other approaches as shown in Fig. 8. In this stage, the total generation is more than the demand. The extra generated power is absorbed by the energy storage systems and stored to use it afterwards. In Fig. 9, the negative powers of the FESS, SMES, EV and UC indicate that they are storing the generated power.

At 40 s, the demand suddenly rises to 0.4 pu whereas the wind and PV power output remains the same. During this period, the total generation (0.33 pu) is less than the total demand (0.4 pu) as only 60% of the generation is utilized to supply the demand. The power outputs of the DEG, FESS, SMES, EV and UC are increased to meet the remaining demand which can be clearly depicted (positive powers of these components) in Fig. 9. In Fig. 9, positive powers of the energy storage devices indicate supply of power when and conversely the negative values signify that they are absorbing power. The coordinated actions of these energy storage components are causing the whole system stable. The figure evidently illustrates that the suggested MSSA-optimized FOAFPIDF offers an efficient damping for frequency deviation in terms of lesser settling time and peak overshoot. This proves the superiority of the suggested controller for sudden variation in input
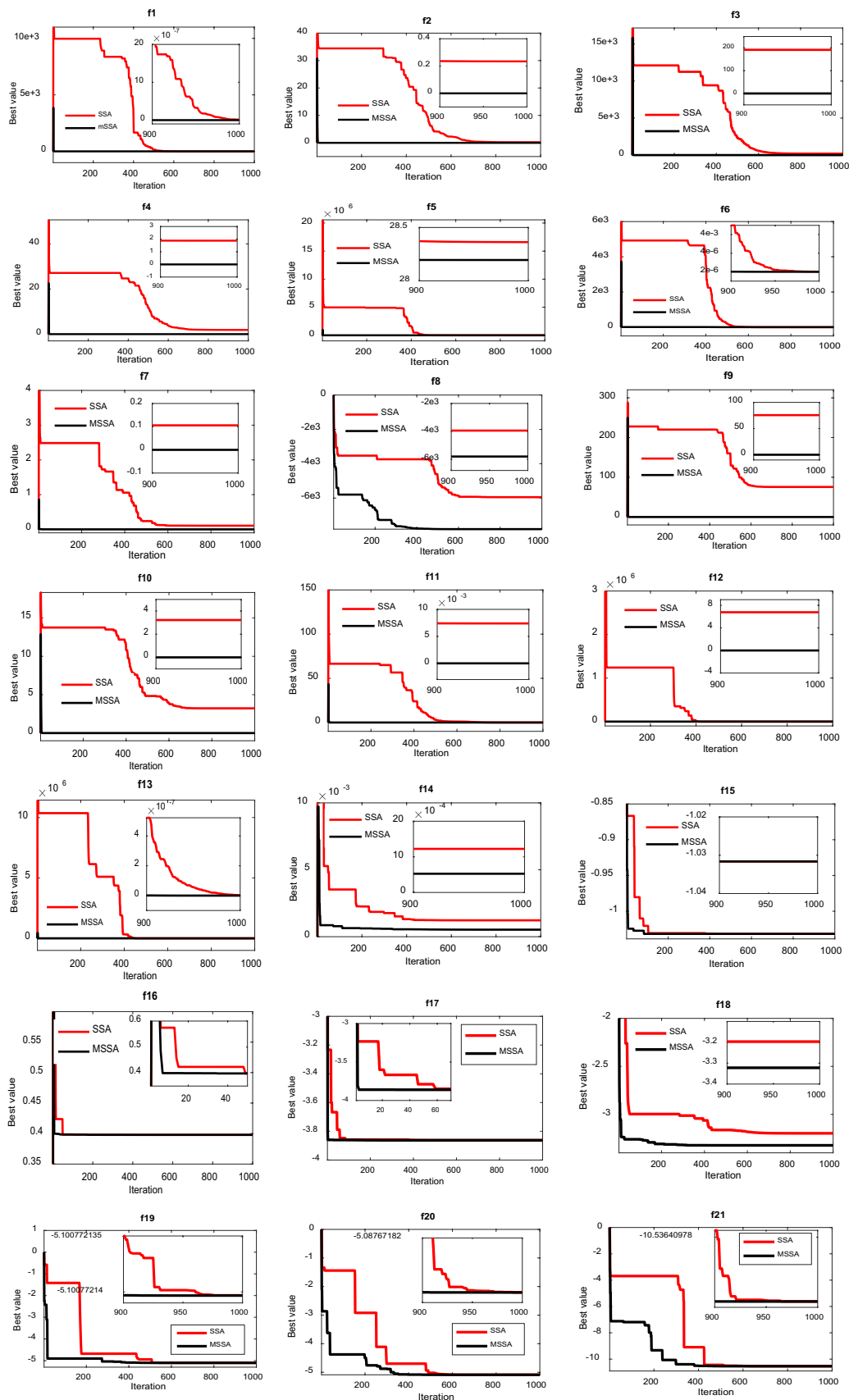
Fig. 6 Comparison of convergence characteristics of the MSSA and the SSA for the benchmark test functions

Table 6 p values of the Wilcoxon's test for a pair-wise comparison of the MSSA vs. SSA, MSSA vs. MFO, MSSA vs. GWO, MSSA vs. PSO, MSSA vs. SCA

	MSSA vs				
	SSA	MFO	GWO	PSO	SCA
f_1	1.2118e−12	1.2118e−12	1.2118e−12	1.2118e−12	1.2118e−12
f_2	1.2118e−12	1.2118e−12	1.2118e−12	1.2118e−12	1.2118e−12
f_3	4.4592e−04	1.2118e−12	1.2118e−12	1.2118e−12	1.2118e−12
f_4	1.2118e-−12	1.2118e−12	1.2118e−12	1.2118e−12	1.2118e−12
f_5	3.9881e−04	1.1077e−06	4.1997e−10	3.0199e−11	3.0199e−11
f_6	3.0199e−11	3.0199e−11	3.0199e−11	3.0199e−11	3.0199e−11
f_7	3.0199e−11	3.0199e−11	3.0199e−11	3.0199e−11	3.0199e−11
f_8	0.0184	6.7650e−05	3.8249e−09	3.0199e−11	3.0199e−11
f_9	1.2118e−12	1.2118e−12	0.0110	1.2118e−12	1.2118e−12
f_{10}	1.2118e−12	1.2118e−12	4.9627e−13	1.2118e−12	1.2118e−12
f_{11}	1.2118e−12	1.2118e−12	0.0419	1.2118e−12	1.2118e−12
f_{12}	3.0199e−11	3.0199e−11	3.0199e−11	3.0199e−11	3.0199e−11
f_{13}	0.0339	0.0615	0.3790	3.0199e−11	3.0199e−11
f_{14}	7.0881e−08	1.5449e−09	0.0051	0.0451	2.1947e−08
f_{15}	7.4474e−09	5.7725e−13	2.1906e−11	2.0270e−11	2.0113e−11
f_{16}	2.8547e−05	NaN	1.2118e−12	0.0154	4.2700e−06
f_{17}	2.4607e−08	5.0943e−13	2.6555e−10	5.2836e−10	2.5315e−10
f_{18}	9.7198e−05	0.3138	4.8880e−04	0.0046	2.8269e−11
f_{19}	4.4592e−04	0.0488	7.3644e−10	0.0038	8.8288e−07
f_{20}	2.5286e−04	6.5677e−04	5.4591e−09	0.0242	0.0016
f_{21}	0.0011	0.0125	8.8349e−07	2.3153e−06	0.0241

Table 7 Parameters of the PID and the FOAFPIDF

	K_P	K_I	K_D	K_{11}	K_{21}	λ	μ	α	J
SSA-PID	0.5068	0.2924	0.7794	–	–	–	–	–	5.3329
MSSA-PID	0.7666	0.4749	0.3836	-	-	-	-	-	5.1948
SSA-FOAFPIDF	0.2543	0.8641	0.1550	0.6819	0.0105	0.9319	0.2776	0.9398	4.3420
MSSA-FOAFPIDF	0.2925	0.8976	0.0577	0.8978	0.6635	0.8795	0.8377	0.7489	4.0846

or load. For rest of the cases, MSSA-based FOAFPIDF is equated with the MSSA-based PID for better illustration.

7.4 Case 2:

The proposed system is simulated with constant PV and wind power output of 0.1 pu and random load fluctuation as shown in Fig. 10. The load varies randomly from 0.08 pu to 0.12 pu throughout the simulation time of 60 s. The frequency deviation responses are provided in Fig. 11.

The figure clearly shows that the FOAFPIDF is superior to PID with regard to the deviations in frequency from its steady-state value which can be certainly observed from the zoomed plot of Fig. 11. This makes a conclusion that the more no. of controlling parameters of the FOAFPIDF controller makes the power system more robust towards varied operating conditions.

7.5 Case 3:

The proposed controller is validated by taking the speculative variations of PV, wind and multi-step variation of load demand as revealed in Fig. 12. The figure depicts a random variation of wind and PV near 0.6 pu and 0.4 pu, respectively. In order to make an equilibrium between generation and demand, the energy storing components supply the surplus amount of power to meet the demand. It is clear from Fig. 13 that MSSA-optimized FOAFPIDF handles the uncertainties in a better way while obtaining the controller parameters making the system stable quicker than that of PID.

The proposed controller enhances the frequency response in terms of peak overshoot than PID controller. The sudden load disturbances have been occurred throughout the simulation time of 60 s. The effective control action of the proposed controller gives rise to the output
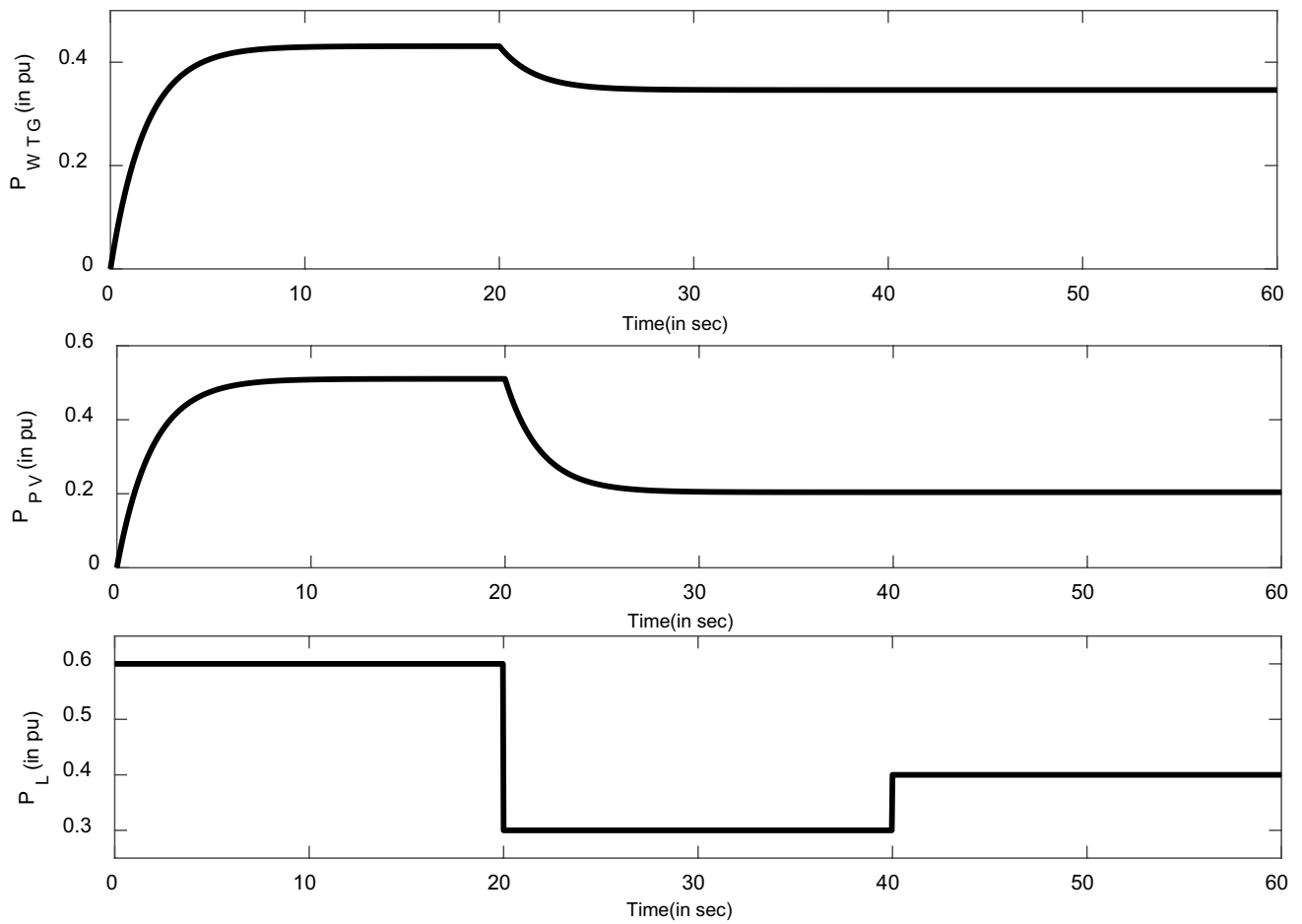
Fig. 7 Single realization of the generated power and load demand (Case 1)
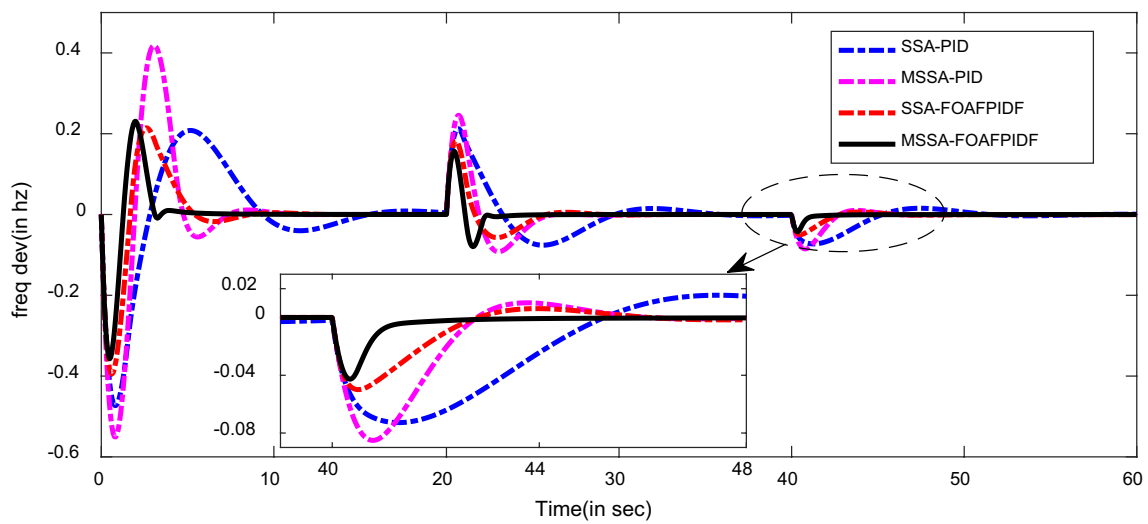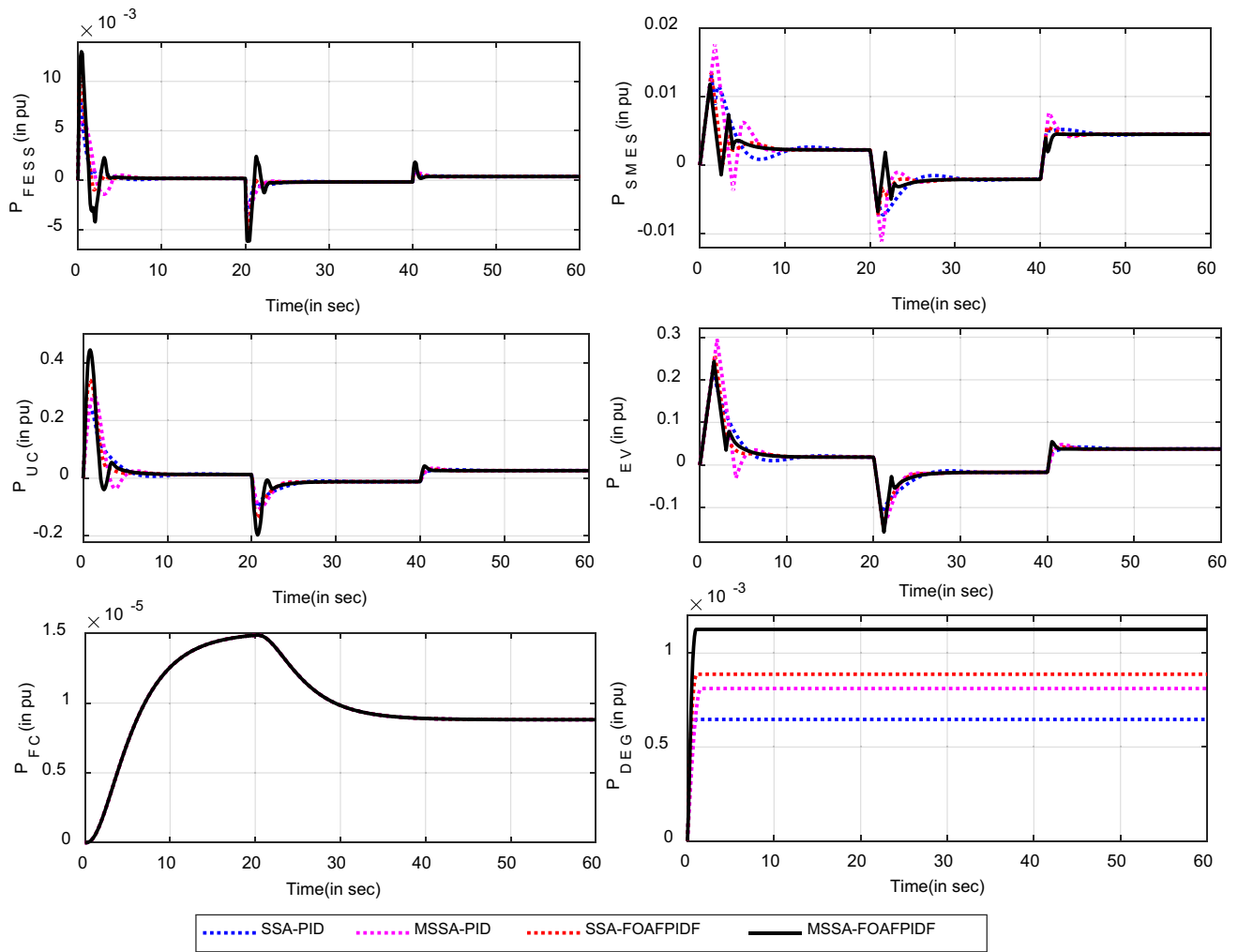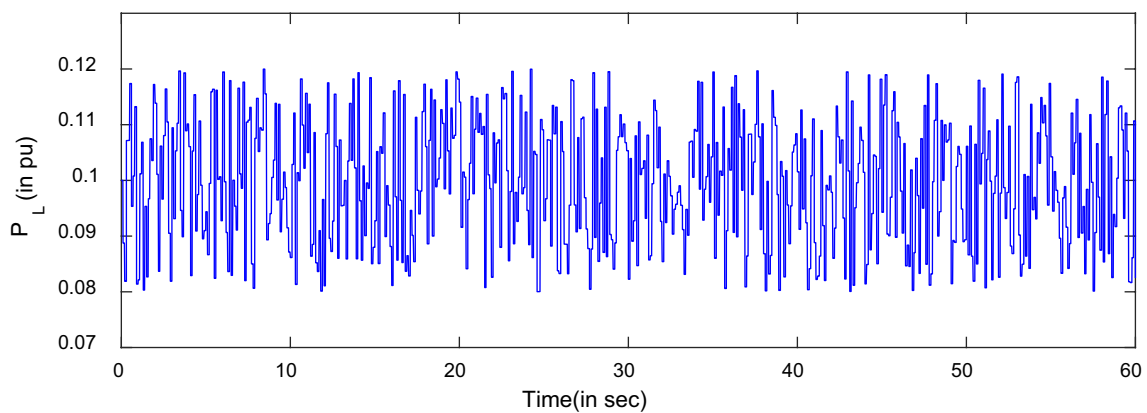

Fig. 8 Frequency deviation with PID and FOAFPIDF (case 1)

Fig.9 Associated powers of components of hybrid power system (Case 1)

Fig. 10 Random load change (Case 2)

powers of DEG, FC and energy storing components to change over to an appropriate value to get the proportion among the generation and demand. The settling time of

the frequency variations is also greatly reduced with the projected FOAFPIDF controller as revealed in Fig. 13.
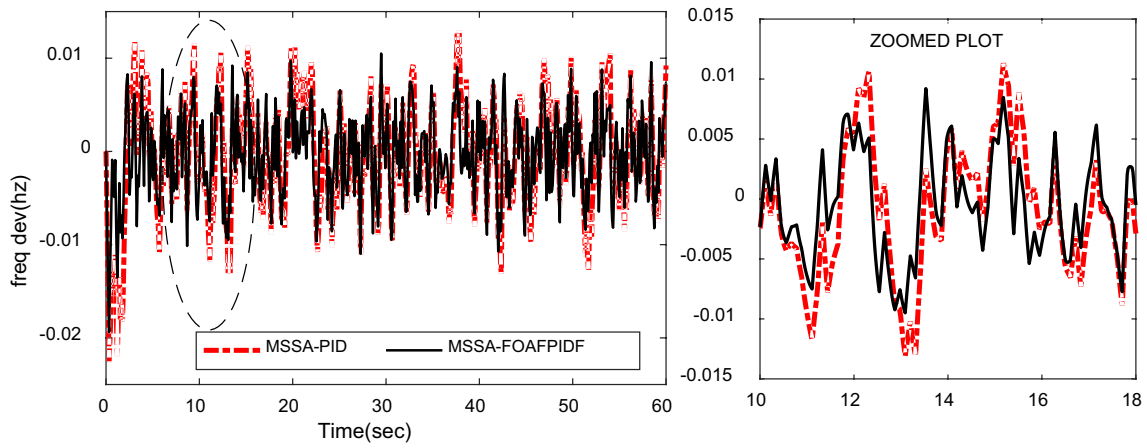
Fig. 11 Frequency deviation with PID and FOAFPIDF (case 2)
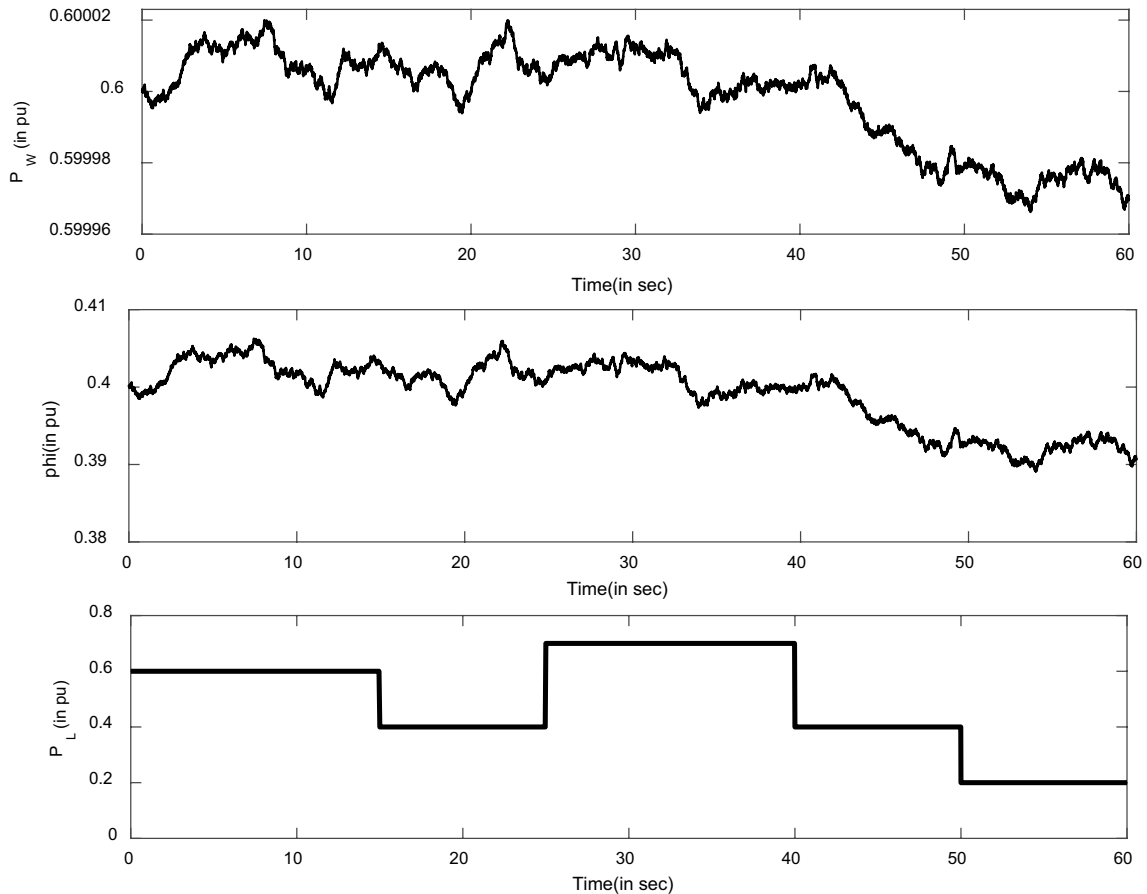
Fig. 12 Single realization of the generated renewable power and the demand (Case 3)

7.6 Case 4

The hybrid power system parameters are varied in the limits as given in Table 8 for evaluating the robustness of FOAFPIDF controller under dynamical changes of the power system due to various environmental impacts or due to abnormal operations. Table 8 reports the percentage change in J which is calculated using notation $\left(\frac{J - J_{no\,min\,al}}{J_{no\,min\,al}}\right) \bullet 100$ for both the raise and reduction in values of HPS parameters like D, M, K_{DEG}, T_{DEG}, K_{FESS}, T_{FESS},
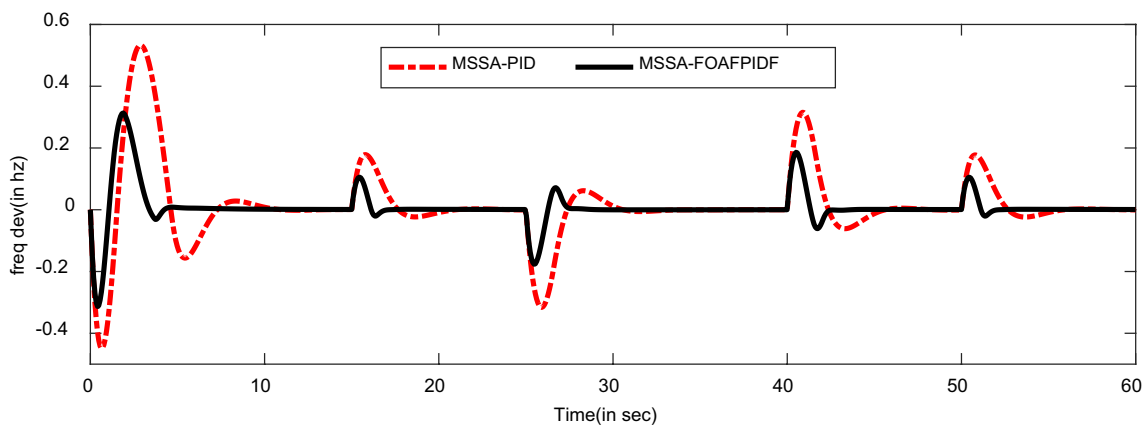
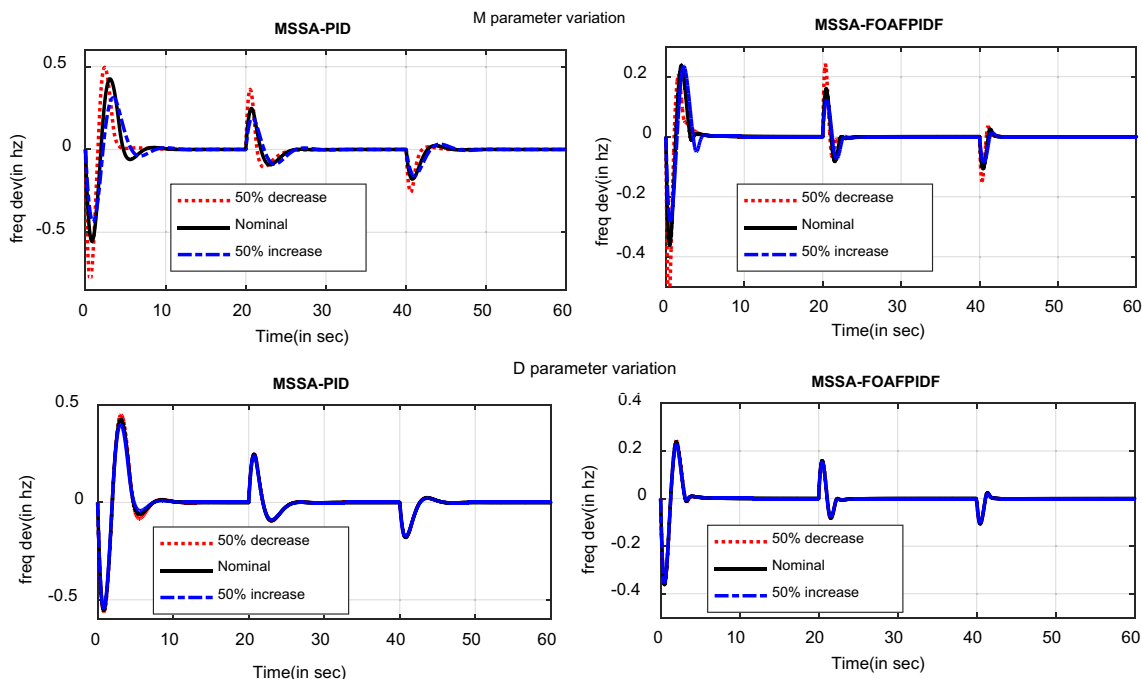**Fig. 13** Frequency deviation with PID and FOAFPIDF (case 3)

Fig.14 Frequency deviation under parameter (*M* & *D*) variations (case 4)

T_{EV}, K_{EV}, τ. It is evident from Table 8 that under varied conditions the FOAFPIDF controller shows reduced percentage change in *J* as compared to PID for all parameters. Figure 14 depicts the grid frequency deviation of MSSA-PID and MSSA-FOAFPIDF for $\pm 50\%$ variation and nominal condition in case of *M* and *D* parameter. It can be seen from Table 8 and Fig. 14 that the system performance degrades when the M parameter is decreased and vice versa. It is also noticed that the effect of D parameter on system performance is negligible as evident from Table 8 and Fig. 14. In all the cases, FOAFPIDF is much more

efficient in tolerating the parameter variations than the PID.

7.7 Case 5:

Case 5 examines the strength of the designed controller in a case where there is a disconnection of any energy storage components. Among all the four energy storage components, FESS and SMES share the lowest power and EV and UC share the maximum of storage power. Thus, one from each group (SMES and EV) has taken for the validation purpose.
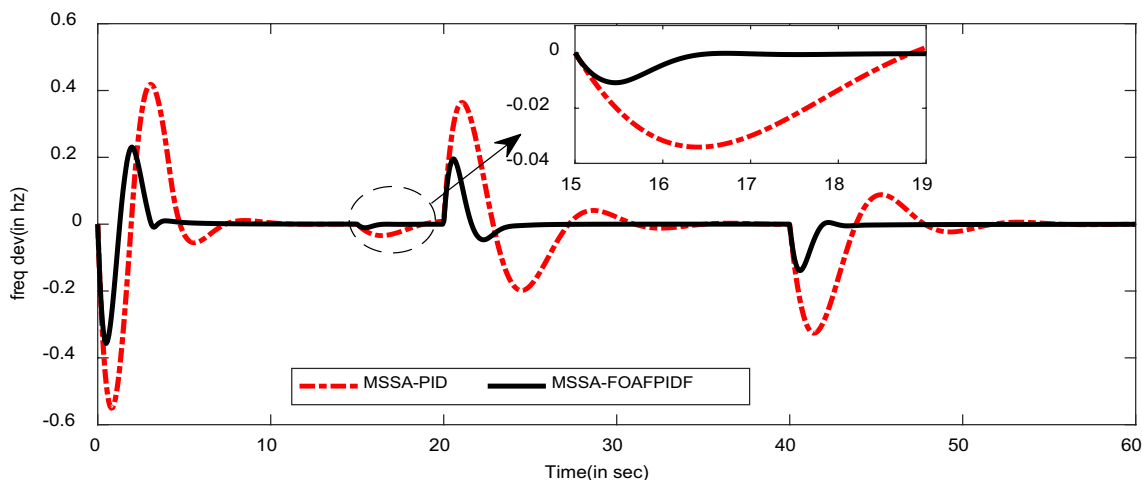
Fig. 15 Frequency deviation with PID and FOAFPIDF (case 5)

At Time = 15 s, SMES and EV are disconnected from the system with the WTG, PV power output and demand as in case 1. Figure 15 shows that the FOAFPIDF controller improves the performance of the studied system in comparison to the PID controller. As can be seen, despite the disconnection of the SMES and EV, our proposed controller is better than that of PID controller in terms of lowering overshoot and faster settling time.

7.8 Case 6:

There is a possibility that the system might undergo certain abnormal conditions during the course of their operation. The classical PID controller is quite simple and works well for linear system. However, when the system contains nonlinearity and uncertainty, the performance of the PID controller may deteriorate and the system might be unstable.

However, FOAFPIDF controller is capable of handling the uncertainty and may maintain stability in presence of uncertainty. Hence, the performance of the MSSA-optimized PID and FOAFPIDF controller is investigated against severe system uncertainty scenarios as given below.

Scenario I: In this scenario, WTG, PV output power becomes zero and UC power reduces by 75% while all the other components operating at their nominal value throughout the simulation time.

Scenario II: In this scenario, demand pattern increases by 50% while UC power reduces to 25% and WTG, PV sources become unavailable simultaneously.

Scenario III: The load demand pattern and EV power output increases by 25% and 50%, respectively, whereas UC power reduces by 75% and WTG, PV power output becomes zero.

Fig. 16 Frequency deviation with PID and FOAFPIDF (case 6)
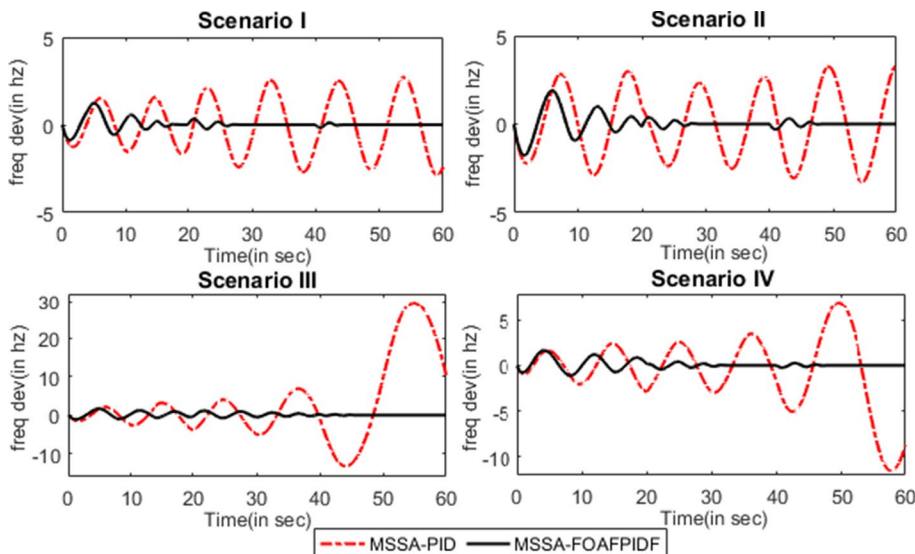
Table 8 (Case 4) Percentage change in j for HPS parameter perturbation

Parameter	Variations	Percentage change in *Jss*	
		PID	FOAFPIDF
M	50% Increase	–3.390	−1.324
	50% Decrease	0.782	0.290
D	50% Increase	−3.683	−1.668
	50% Decrease	0.060	2.639
K_{DEG}	50% Increase	7.475	2.388
	50% Decrease	−2.797	−1.526
T_{DEG}	50% Increase	7.654	2.621
	50% Decrease	−3.001	−1.829
K_{FESS}	50% Increase	6.185	1.427
	50% Decrease	−1.835	−0.608
T_{FESS}	50% Increase	7.629	2.574
	50% Decrease	−2.918	−1.671
K_{EV}	50% Increase	22.039	1.206
	50% Decrease	16.441	6.057
T_{EV}	50% Increase	9.660	1.457
	50% Decrease	−7.061	−3.557
τ	50% Increase	9.889	4.112
	50% Decrease	−4.464	−3.086

Scenario IV: The WTG, PV power output increases by 50%, UC power reduces by 80% and demand increases by 25%.

The system frequency deviation characteristics for the above scenarios are shown in Fig. 16. For all the above scenarios, the frequency deviation characteristics severely oscillate and the system becomes unstable with the PID controller. However, stability of the system is eventually stored with the designed FOAFPIDF.

7.9 Case 7:

The credibility of the proposed MSSA-optimized FOAFPIDF controller is also investigated in an extensively employed test system (Ali and Abd-Elazim 2011; Panda et al. 2013; Panda and Yegireddy 2013; Sahu et al. 2015). Two identical FOAFPIDF structures are taken for each area owing to their identical nature. A sudden rise in demand of 10% is assumed at $t = 0$ s in area-1 and the FOAFPIDF parameters are found to be, $K_P = 0.5281$, $K_I = 0.4548$, $K_D = 0.8265$, $k_{11} = 0.8932$, $k_{21} = 0.1400$, $\lambda = 0.9989$, $\mu = 0.5933$, $\alpha = 0.8268$.

The performance of proposed controller is equated with traditional and some latest optimization approaches like Ziegler Nichols (ZN) (Ali and Abd-Elazim 2011), Genetic

Table 9 ITAE values for the different controllers

Performance/Technique: Control Structure	ITAE
Conventional ZN: PI Ali and Abd-Elazim (2011)	3.5795
GA: PI Ali and Abd-Elazim(2011)	2.7475
BFOA: PI Ali and Abd-Elazim (2011)	1.8379
PSO: PI Panda et al. (2013)	1.2142
hBFOA-PSO: PI Panda et al. (2013)	1.1865
NSGA-II: PI Panda and Yegireddy (2013)	1.1785
NSGA-II: PIDF Sahu et al. (2015)	0.387
PS: Fuzzy PI Sahu et al. (2015)	0.6334
PSO: Fuzzy PI Sahu et al. (2015)	0.4470
Proposed MSSA-based FOAFPIDF	0.1911

Algorithm (GA) (Ali and Abd-Elazim 2011), Bacterial Foraging Optimization Algorithm (BFOA) (Ali and Abd-Elazim 2011), Particle Swarm Optimization (PSO) (Panda et al. 2013), hybrid BFOA-PSO (Panda et al. 2013), NSGA-II-based PI controller (Panda and Yegireddy 2013), NSGA-II-optimized PIDF controller (Sahu et al. 2015) as well as Pattern Search (PS), PSO-optimized fuzzy PI controllers (Sahu et al. 2015). Table 9 provides the objective function value.

Table 9 shows that minimum integral time absolute error (ITAE) value is attained with MSSA tuned FOAFPIDF as than some lately projected AGC schemes. The frequency deviation of area-1 for the same is given in Fig. 17 which shows that the suggested method is better than some newly suggested automatic generation control methods.

8 Conclusion

A novel LFC method is proposed in this paper to control frequency of a hybrid power system incorporated with numerous renewable energies and storage components as well as EVs. To tune the controller gains, a modified SSA technique is suggested. The superiority of proposed MSSA technique over original SSA, MFO, GWO, PSO and SCA techniques has been shown for benchmark test functions using statistical analysis. The results show the effectiveness of the proposed approach in minimizing the grid frequency oscillation compared to a PID controller. Robustness of the FOAFPIDF controller under significantly varied parameter is also established. EV's gain has taken as constant in this paper. But when the battery's state of charge (SOC) is taken into consideration, EV's gain becomes time-varying and may have an impact on the controller action. Further research in this direction can be made to include EVs SOC.
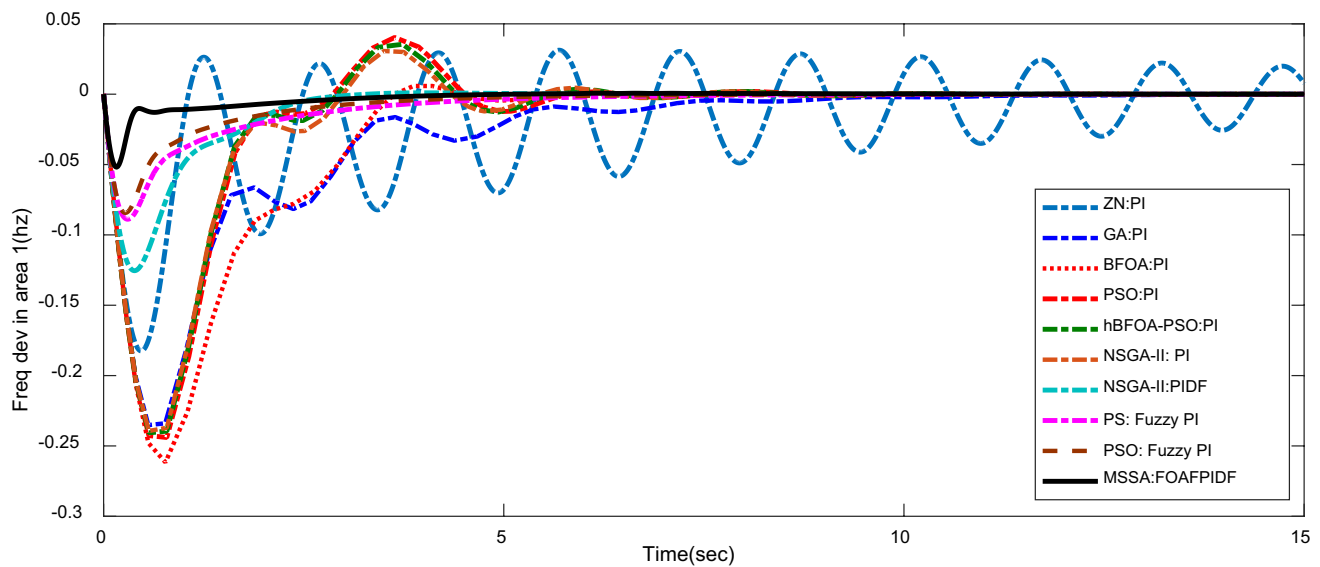
Fig. 17 Frequency deviation of area-1 (Case 7)

References

Agrawal, B. L., Anderson, P. M., Concordia, C., Farmer, R. G., Fouad, A. A., Kundur, P., et al. (1999). Damping representation for power system stability studies. *IEEE Transactions on Power Systems., 14*(1), 151–157.

Ali, E. S., & Abd-Elazim, S. M. (2011). Bacteria foraging optimization algorithm based load frequency controller for interconnected power system. *International Journal of Electrical Power & Energy Systems, 33*(3), 633–638.

Ali, R., Mohamed, T. H., Qudaih, Y. S., & Mitani, Y. (2014). A new load frequency control approach in an isolated small power systems using coefficient diagram method. *International Journal of Electrical Power & Energy Systems, 56,* 110–116.

Alomoush, M. I. (2010). Load frequency control and automatic generation control using fractional-order controllers. *Electrical Engineering.,, 91*(7), 357–368.

Chaturvedi, K. T., Pandit, M., & Srivastava, L. (2009). Particle swarm optimization with time varying acceleration coefficients for non-convex economic power dispatch. *International Journal of Electrical Power & Energy Systems, 31*(6), 249–257.

Cuevas, E., Echavarria, A., & Ramirez-Ortegon, M. A. (2014). An optimization algorithm inspired by the states of matter that improves the balance between exploration and exploitation. *Applied Intelligence, 40*(2), 256–272.

Datta, M., & Senjyu, T. (2013). Fuzzy control of distributed PV inverters/energy storage systems/electric vehicles for frequency regulation in a large power system. *IEEE Transactions on Smart Grid., 4*(1), 479–488.

Debbarma, S., & Dutta, A. (2016a). Utilizing electric vehicles for LFC in restructured power systems using fractional order controller. *IEEE Transactions on Smart Grid., 8*(6), 1–11.

Debbarma, S., & Dutta, A. (2016b). Utilizing electric vehicles for LFC in restructured power systems using fractional order controller. *IEEE Transactions on Smart Grid., 8*(6), 2554–2564.

Fereidouni, A., Masoum, M. A., & Moghbel, M. (2015). A new adaptive configuration of PID type fuzzy logic controller. *ISA Transactions., 56,* 222–240.

Kennel, F., Gorges, D., & Liu, S. (2013). Energy management for smart grids with electric vehicles based on hierarchical MPC. *IEEE Transactions on Industrial Informatics, 9*(3), 1528–1537.

Ko, K. S., & Sung, D. K. (2017). The effect of EV aggregators with time-varying delays on the stability of a load frequency control system. *IEEE Transactions on Power Systems., 33*(1), 1–12.

Lee, D. J., & Wang, L. (2008). Small-signal stability analysis of an autonomous hybrid renewable energy power generation/energy storage system part-I: Time-domain simulations. *IEEE Transactions on Energy Conversion, 23*(1), 311–320.

Mamdani, E. H. (1974). Applications of fuzzy algorithms for simple dynamic plant. *Proceedings of the Institution of Electrical Engineers.,, 121*(12), 1585–1588.

Masuta, T., & Yokoyama, A. (2012). Supplementary load frequency control by use of a number of both electric vehicles and heat pump water heaters. *IEEE Transactions on Smart Grid., 3*(3), 1253–1262.

Mirjalili, S. (2015). Moth-flame optimization algorithm: A novel nature-inspired heuristic paradigm. *Knowledge-Based Systems., 89,* 228–249.

Mirjalili, S. (2016). SCA: A sine cosine algorithm for solving optimization problems. *Knowledge-Based Systems., 96,* 120–133.

Mirjalili, S., Gandomi, H., Mirjalili, S., Saremi, S., Faris, H., & Mirjalili, S. M. (2017). Salp swarm algorithm: A bio-inspired optimizer for engineering design problems. *Advances in Engineering Software.,, 114,* 163–191.

Mirjalili, S., Mirjalili, S. M., & Lewis, A. (2014). Grey wolf optimizer. *Advances in Engineering Software., 69,* 46–61.

Padhy, S., Panda, S., & Mahapatra, S. (2017). A modified GWO technique based cascade PI-PD controller for AGC of power systems in presence of plug in electric vehicles. *Engineering Science and Technology, an International Journal, 20*(2), 427–442.

Pahasa, J., & Ngamroo, I. (2015). PHEVs bidirectional charging/discharging and SoC control for microgrid frequency stabilization using multiple MPC. *IEEE Transactions on Smart Grid., 6*(2), 526–533.

Pan, I., & Das, S. (2015). Kriging based surrogate modeling for fractional order control of microgrids. *IEEE Transactions on Smart Grid., 6*(1), 36–44.

Pan, I., & Das, S. (2016a). Fractional order AGC for distributed energy resources using robust optimization. *IEEE Transactions on Smart Grid., 7*(5), 2175–2186.

Pan, I., & Das, S. (2016b). Fractional order fuzzy control of hybrid power system with renewable generation using chaotic PSO. *ISA Transactions, 62,* 19–29.

Panda, S., Mohanty, B., & Hota, P. K. (2013). Hybrid BFOA–PSO algorithm for automatic generation control of linear and nonlinear interconnected power systems. *Applied Soft Computing., 13*(12), 4718–4730.

Panda, S., & Yegireddy, N. K. (2013). Automatic generation control of multi-area power system using multi-objective non-dominated sorting genetic algorithm-II. *International Journal of Electrical Power & Energy Systems., 53,* 54–63.

Pham, T. N., Nahavandi, S., Hien, L. V., Trinh, H., & Wong, K. P. (2017). Static output feedback frequency stabilization of time-delay power systems with coordinated electric vehicles state of charge control. *IEEE Trans on Power Systems., 32*(5), 3862–3874.

Pothiya, S., & Issarachai, N. (2008). Optimal fuzzy logic-based PID controller for load–frequency control including superconducting magnetic energy storage units. *Energy Conversion and Manage, 49*(10), 2833–2838.

Ranganayakulu, R., Babu, G. U., Rao, A. S., & Patle, D. S. (2016). A comparative study of recent fractional order $PI^{\lambda}/PI^{\lambda}D^{\mu}$ tuning rules for stable first order plus time delay processes. *Separation Technologies in Chemical, Biochemical, Petroleum and Environmental Engineering., 15,* 136–152.

Ray, P., Mohanty, S., & Kishor, N. (2010). Small-signal analysis of autonomous hybrid distributed generation systems in presence of Ultra capacitor and tie-line operation. *Journal of Electrical Engineering., 61*(4), 205–214.

Ray, P. K., Mohanty, S. R., & Kishor, N. (2011). Proportional–integral controller based small-signal analysis of hybrid distributed generation systems. *Energy Conversion and Management, 52*(4), 1943–1954.

Sahu, R. K., Panda, S., & Sekhar, G. C. (2015). A novel hybrid PSO-PS optimized fuzzy PI controller for AGC in multi area interconnected power systems. *International Journal of Electrical Power & Energy Systems., 64,* 880–893.

Savran, A., & Kahraman, G. (2014). A fuzzy model based adaptive PID controller design for nonlinear and uncertain processes. *ISA Transactions., 53*(2), 280–288.

Senjyu, T., Nakaji, T., Uezato, K., & Funabashi, T. (2005). A hybrid power system using alternative energy facilities in isolated island. *IEEE Transactions on Energy Conversion., 20*(2), 406–414.

Taher, S. A., Fini, M. H., & Aliabadi, S. F. (2014). Fractional order PID controller design for LFC in electric power systems using imperialist competitive algorithm. *Ain Shams Engineering Journal.,, 5*(1), 121–135.

Vachirasricirikul, S., & Ngamroo, I. (2014). Robust LFC in a smart grid with wind power penetration by coordinated V2G control and frequency controller. *IEEE Transactions on Smart Grid, 5*(1), 371–380.

Woo, Z. W., Chung, H. Y., & Lin, J. J. (2000). A PID type fuzzy controller with self-tuning scaling factors. *Fuzzy Sets and Systems, 115*(2), 321–326.

Yao, X., Liu, Y., & Lin, G. (1999). Evolutionary programming made faster. *IEEE Transactions on Evolutionary Computation., 3*(2), 82–102.

Zhang, J., & Xu, H. (2017). Online identification of power system equivalent inertia constant. *IEEE Transactions on Industrial Electronics., 64*(10), 8098–8107.